iScience

CellPress
OPEN ACCESS

Article

Drp1 SUMO/deSUMOylation by Senp5 isoforms influences ER tubulation and mitochondrial dynamics to regulate brain development

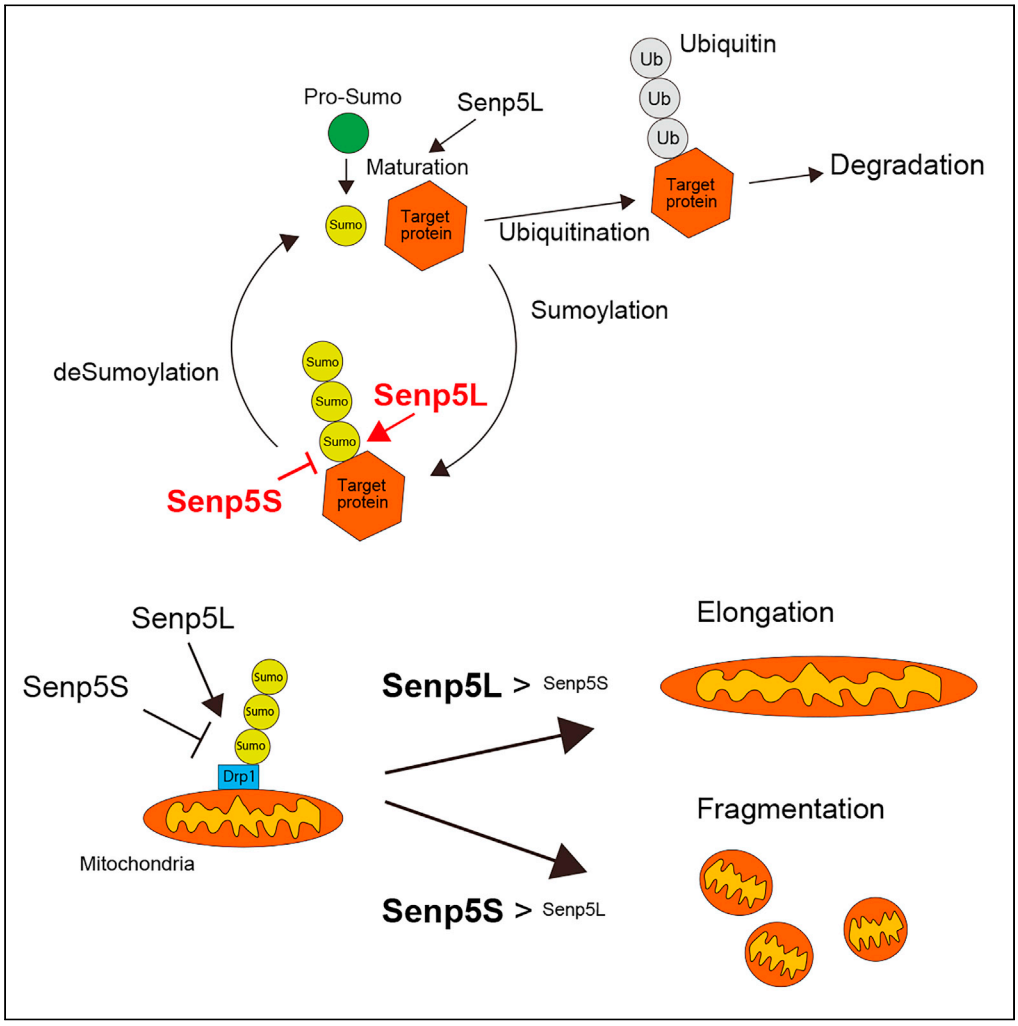

Seiya Yamada, Ayaka Sato, Naotada Ishihara, Hiroki Akiyama, Shin-ichi Sakakibara

h-akiyama@kurenai.waseda.jp (H.A.)
sakakiba@waseda.jp (S.-i.S.)

Highlights

We identified the novel peptidase-activity lacking splice valiant of Senp5, or Senp5S

The conventional Senp5 (Senp5L) and Senp5S competitively regulate target SUMOylation

Senp5L/S inhibits/promotes mitochondrial fission via the control of Drp1 SUMOylation

Balanced expression of Senp5L/S and Drp1 SUMOylation are required for corticogenesis

Yamada et al., iScience 24, 103484
December 17, 2021
https://doi.org/10.1016/j.isci.2021.103484

iScience

CellPress
OPEN ACCESS

Article

Drp1 SUMO/deSUMOylation by Senp5 isoforms influences ER tubulation and mitochondrial dynamics to regulate brain development

Seiya Yamada,[1] Ayaka Sato,[1] Naotada Ishihara,[2] Hiroki Akiyama,[1,3,*] and Shin-ichi Sakakibara[1,3,4,*]

SUMMARY

Brain development is a highly orchestrated process requiring spatiotemporally regulated mitochondrial dynamics. Drp1, a key molecule in the mitochondrial fission machinery, undergoes various post-translational modifications including conjugation to the small ubiquitin-like modifier (SUMO). However, the functional significance of SUMOylation/deSUMOylation on Drp1 remains controversial. SUMO-specific protease 5 (Senp5L) catalyzes the deSUMOylation of Drp1. We revealed that a splicing variant of Senp5L, Senp5S, which lacks peptidase activity, prevents deSUMOylation of Drp1 by competing against other Senps. The altered SUMOylation level of Drp1 induced by Senp5L/5S affects mitochondrial morphology probably through controlling Drp1 ubiquitination and tubulation of the endoplasmic reticulum. A dynamic SUMOylation/deSUMOylation balance controls neuronal polarization and migration during the development of the cerebral cortex. These findings suggest a novel role of post-translational modification, in which deSUMOylation enzyme isoforms competitively regulate mitochondrial dynamics via Drp1 SUMOylation levels, in a tightly controlled process of neuronal differentiation and corticogenesis.

INTRODUCTION

The small ubiquitin-like modifier (SUMO) is a post-translational modifier that influences multiple cellular processes such as protein trafficking, protein stability, transcriptional activation/repression, DNA repair, cell-cycle progression, immune response, and dendritic spinogenesis (Khayachi et al., 2018; Pichler et al., 2017; Verma et al., 2018; Zhao, 2018). SUMOylation is achieved through a cascade of three enzymatic reactions comprising a SUMO-activating enzyme (E1), a conjugating enzyme (E2), and SUMO ligases (E3) (Pichler et al., 2017). Deconjugation or deSUMOylation is mediated by proteases including sentrin/SUMO-specific proteases (Senps) (Hickey et al., 2012). SUMOylation/deSUMOylation is indispensable for neural development (Kang et al., 2010; Lomeli and Vazquez, 2011; Sharma et al., 2013). The components of the SUMOylation machinery, including SUMO1–3 and a SUMO-conjugating enzyme E2 (Ubc9), are abundantly expressed in neural stem/progenitor cells (NSPCs) and immature migrating neurons during mouse brain development (Hasegawa et al., 2014).

Cell division of NSPCs and subsequent migration of neuronal progenies are strictly controlled spatiotemporally during mammalian brain development. Differentiating neurons are classified into stages 1–5 based on their *in vitro* morphological characteristics (Banker, 2018; Takano et al., 2019). Neurons extend filopodia (stage 1) to form multiple immature neurites (stage 2). One of the immature neurites becomes an axon (stage 3), while the others develop into dendrites (stage 4). Dendritic spines are then established (stage 5). In the embryonic cerebral cortex, the newborn neurons migrate radially toward the cortical plate (CP) while undergoing a sequential morphological transformation from multipolar (stages 1 and 2) to bipolar. This occurs within the subventricular zone (SVZ) and lower area of the intermediate zone (Hansen et al., 2017). The trailing process of a bipolar cell becomes an axon; the multipolar to bipolar transition is a polarity establishment process corresponding to stage 3. The leading processes develop into dendrites after the cell reaches its destination (stage 4). Subsequently, dendritic spines are established (stage 5) to enable the synaptic transmission within neural circuits (Hansen et al., 2017). Dysregulation or failure of polarity formation in migrating neurons causes severe brain malformation and psychiatric disorders such as epilepsy and mental retardation (Hansen et al., 2017; Represa, 2019).

[1]Laboratory for Molecular Neurobiology, Graduate School of Human Sciences, Faculty of Human Sciences, Waseda University, Tokorozawa, Saitama 359-1192, Japan

[2]Department of Biological Sciences, Graduate School of Science, Osaka University, Toyonaka, Osaka 560-0043, Japan

[3]Advanced Research Center for Human Sciences, Waseda University, Tokorozawa, Saitama 359-1192, Japan

[4]Lead contact

*Correspondence: h-akiyama@kurenai.waseda.jp (H.A.), sakakiba@waseda.jp (S.-i.S.)

https://doi.org/10.1016/j.isci.2021.103484

Mitochondrial fission and fusion play an essential role in cellular function and maintenance, especially as neurons form long processes. Cytosolic dynamin-related protein 1 (Drp1) gets recruited to the outer mitochondrial membrane and oligomerizes to activate GTP-dependent mitochondrial fission (Adachi et al., 2020; Bertholet et al., 2016). Drp1 deficiency impedes mitochondrial fission and induces mitochondrial aggregates, which disturb proper neural development, neuronal fate commitment, neurite extension, dendrite development, and synapse formation (Ishihara et al., 2009; Iwata et al., 2020). In humans, the dominant-negative allele of the *DRP1* gene causes a broad range of abnormalities such as brain malformation and optic atrophy, leading to early neonatal death (Waterham et al., 2007). These findings establish the importance of Drp1-mediated regulation of mitochondrial dynamics in brain development.

The mechanism of Drp1-mediated mitochondrial fission has been established (Giacomello et al., 2020) and SUMO-conjugation sites in Drp1 are identified (Figueroa-Romero et al., 2009); however, the mechanism of Drp1 SUMOylation-mediated mitochondrial dynamics remains unclear (Guo et al., 2013; Kang et al., 2010). Moreover, we find no reports showing the detailed machinery for SUMOylation-dependent regulation of brain development. Here, we report that the novel Senp5 isoform, which lacks peptidase activity, prevents deSUMOylation in a competitive manner. We further demonstrated its *in vitro* and *in utero* involvement in neuronal development during corticogenesis.

RESULTS

Identification of the Senp5S isoform

Previous studies reported that the mouse *Senp5* gene encoded a single 749-amino-acid (aa) protein of a molecular mass of 97 kDa (Figure 1A) (Kim et al., 2015). However, our database searches of public cDNA sequences (GenBank, and dbEST containing the single pass cDNA sequences and Expressed Sequence Tags) predicted the existence of other *Senp5* isoforms that lack the C-terminal catalytic domain. We performed RT-PCR using mRNA isolated from early embryonic (E12) and adult mouse brains and confirmed the expression of *Senp5* short isoforms, which were generated by alternative splicing of *Senp5* transcript. We designated one of these short isoforms as Senp5S and the conventional isoform as Senp5L (Figure 1A). Senp5S was predicted to have a molecular mass of 72 kDa and lack the enzymatic catalytic center (Cys 707) critical for peptidase activity. A comparable short isoform of Senp5 lacking most of the residues of the C-terminal catalytic triad (629–674 aa) is known in humans (Q96HI0-2). Quantitative PCR (qPCR) analysis indicated that *Senp5L* and *Senp5S* mRNAs are concurrently expressed during embryonic stages and are gradually upregulated throughout the brain development (Figures 1B and 1C). Consistently, western blot analysis with pan-Senp5 antibody that was validated by using shRNA (Figure 1D; detailed information on shRNA will be described in the later section) revealed the developmentally regulated expression of Senp5 isoform proteins (Figure 1E). The slower migrating protein of a size of ~100 kDa, which presumably corresponds to Senp5L, was detected throughout the brain development. However, the putative Senp5S was barely detectable in the E12 brain but rapidly increased in the late embryonic and postnatal periods, as doublet bands of ~75 kDa (Figure 1E). Western blotting of cultured NSPCs and differentiating cortical neurons cultured for 3 days *in vitro* (div) showed that NSPCs solely express Senp5L, whereas immature neurons start to express Senp5S (Figure 1E). We concluded that Senp5L is a dominant form in the early embryonic stages, E12–E14 when active neurogenesis occurs, whereas Senp5S becomes upregulated during the differentiation stage and becomes the dominant form in postnatal and adult brains.

Senp5S promotes global SUMOylation

To test whether Senp5S affects protein deSUMOylation, we monitored global SUMOylation in HEK293T cells expressing enhanced green fluorescent protein fused to Senp3 (EGFP-Senp3), -Senp5L, or -Senp5S and hemagglutinin (HA)-SUMO3 or HA-SUMO1. SUMOs are covalently attached to the ε-amino groups of lysine residues in all target proteins (Varejão et al., 2020). SUMO3 but not SUMO1 includes a conserved sequence, ΨKxD/E, for SUMOylation (ψ; large hydrophobic amino acid, x; any amino acid). Thus, SUMO3 can form a polySUMO chain on the target protein (Saitoh and Hinchey, 2000; Tatham et al., 2001). In control EGFP-expressing cells, many HA-SUMO3-conjugated proteins were detected as ladder bands with high molecular weight (Figure 2A). These SUMO3-conjugated proteins were dramatically reduced or even diminished by exogenous expression of Senp3 or Senp5L, thus confirming the deSUMOylation activity. In contrast, Senp5S substantially increased SUMO3-conjugated proteins compared with EGFP as a control. This Senp5S-mediated SUMOylation was almost abolished by co-transfection of Senp3 or Senp5L, which suggested the competitive nature of Senp5S and Senp5L. Same results were also observed in Neuro2a cells (Figure S1B). On the other hand, although the content of HA-SUMO1-conjugated proteins seemed

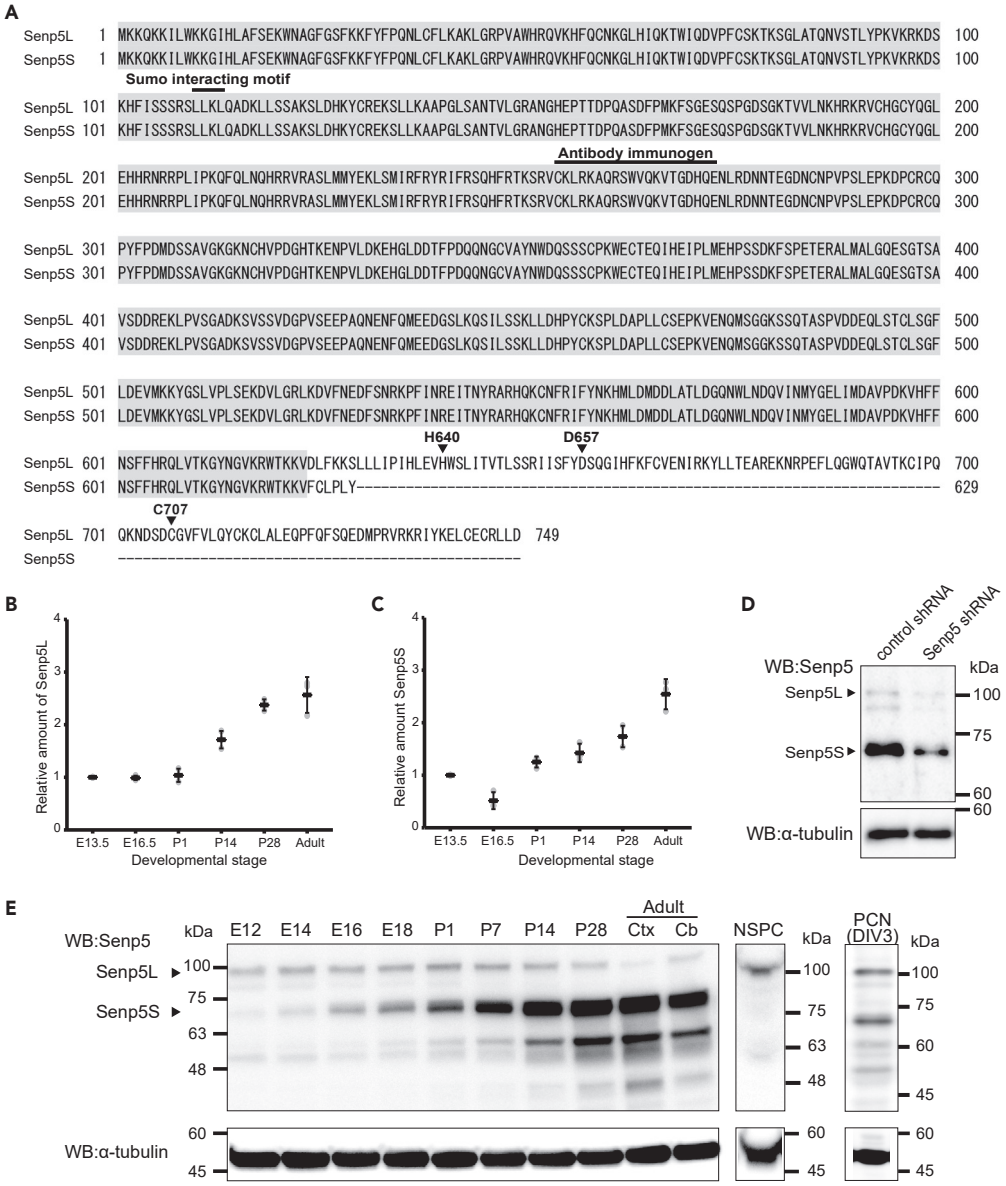

Figure 1. Identification of Senp5S isoform

(A) The deduced amino acid sequences of mouse Senp5L and Senp5S. Identical amino acids are highlighted. Gaps in the alignment are indicated by dashes. Arrowhead denotes the catalytic center Cys-707 necessary for peptidase activity. His-640, Asp-657, and Cys-707 constitute the catalytic triad for cysteine protease. The N-terminal LLKL sequence (110–113) is the SUMO-interacting motif. Only Senp5S lacks the C-terminal catalytic center, although both isoforms have the N-terminal SUMO-interacting motif.

(B and C) Developmental changes in *Senp5L* (B) and *Senp5S* (C) mRNA expression in the mouse cerebral cortex by qPCR analysis. Gray dots represent three independent experiments normalized to the corresponding β-actin mRNA. Mean ± SD are also shown.

(D) PCNs prepared from mouse embryonic brains were electroporated with *Senp5* shRNA or non-targeting control shRNA and cultured for 3 div. Immunoblot with anti-Senp5 or α-tubulin antibody demonstrated the suppression of endogenous protein expression of Senp5L and Senp5S.

(E) Developmental changes in Senp5L/5S protein expression in the mouse brain. Total protein extracts were prepared from the whole brains (E12–P28), adult cerebral cortex (ctx), or adult cerebellum (cb) and subjected to immunoblotting with anti-Senp5 antibody (left panel). Protein lysate from primary cultured neural stem/precursor cells (NSPC) or primary cultured cortical neurons (PCN) at 3 div was also analyzed by immunoblot (middle and right panels). The blots were reprobed with anti-α-tubulin antibody (bottom panels) to examine protein loading quantitatively.

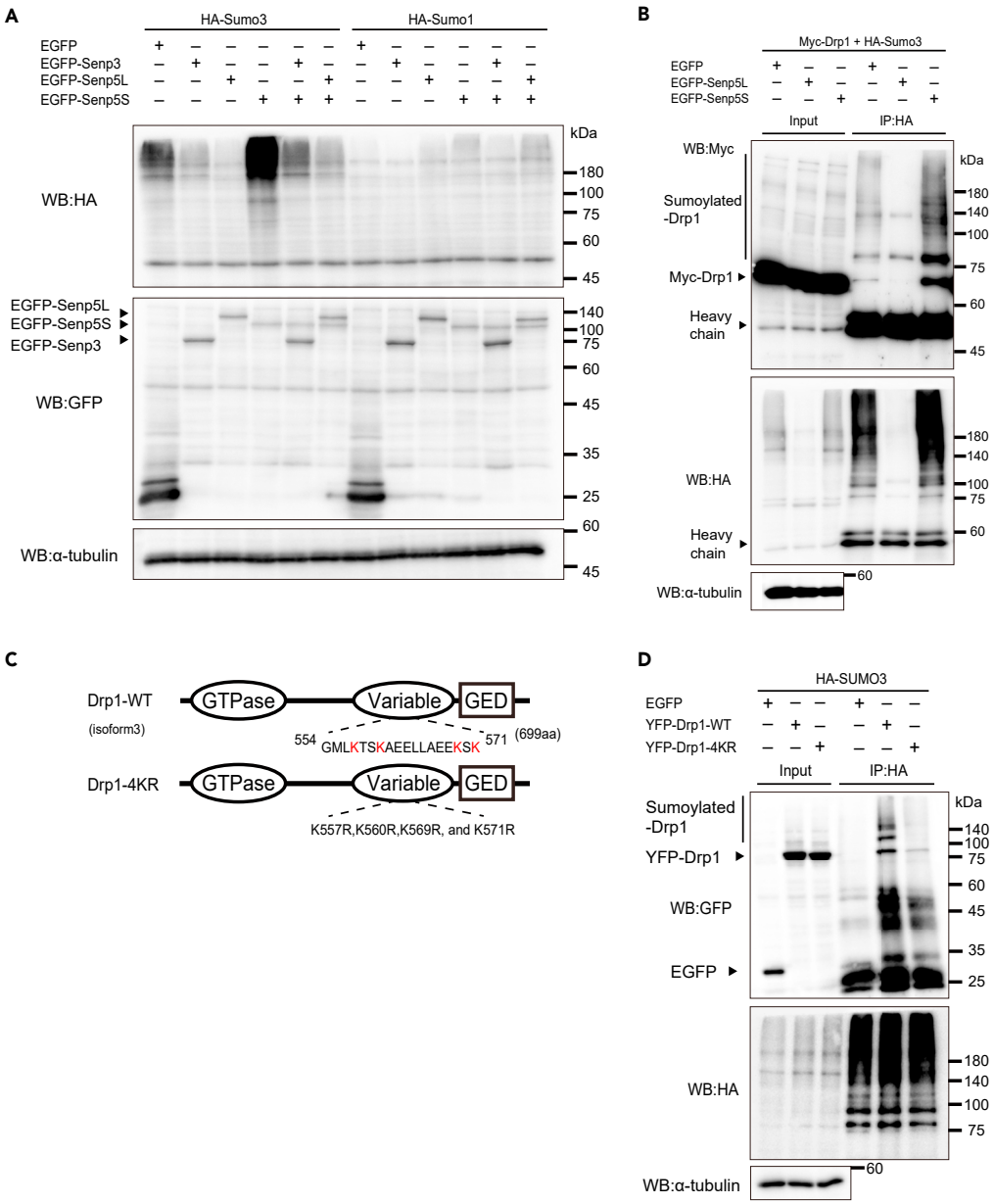

Figure 2. Senp5S competes with other Senps and promotes SUMOylation

(A) Global SUMO3-ylation levels changed by expression of Senp5 isoforms. HEK293T cells were transfected with EGFP, EGFP-Senp3, EGFP-Senp5L, or EGFP-Senp5S along with HA-SUMO3 or HA-SUMO1, followed by immunoblotting with anti-HA (upper panel), anti-GFP (middle panel), or anti-α-tubulin (bottom panel).

(B) Effect of Senp5L and Senp5S expression on SUMO3-ylation of Drp1. HEK293T expressing EGFP, EGFP-Senp5L, or EGFP-Senp5S along with Myc-Drp1 and HA-SUMO3 were immunoprecipitated (IP) with anti-HA antibody. Total cell lysates (input) or IP samples were analyzed by immunoblotting with anti-Myc (upper panel) and anti-HA (bottom panel). Immunoblot with an α-tubulin antibody as a loading control. SUMOylated-Drp1 is indicated by the perpendicular line. Heavy chain, immunoglobulin heavy chain of the HA antibody.

(C) Domain structures of wild-type Drp1 (Drp1-WT) and a non-SUMOylatable Drp1 mutant (Drp1-4KR). The D-octadecapeptide sequence, comprising 18 amino acid residues (554–571) encompassing in the variable domain, is indicated. Drp1-4KR was created by substituting four SUMO-acceptor lysine residues (*red*) in the D-octadecapeptide with arginine residues. Oval and rectangle indicate GTPase activity domain and GTPase effector domain (GED), respectively.

(D) Drp1 was SUMO3-ylated through the D-octadecapeptide sequence. HEK293 cells were co-transfected with HA-SUMO3, p14-Arf, Ubc9, and GFP, YFP-Drp1-WT or YFP-Drp1-4KR, then immunoprecipitated with anti-HA. Cell lysates (input) or IP samples were analyzed by immunoblotting with anti-GFP (top panel) or anti-HA (bottom panel). Immunoblot with an α-tubulin antibody as a loading control. SUMOylated-Drp1 is indicated by the perpendicular line.

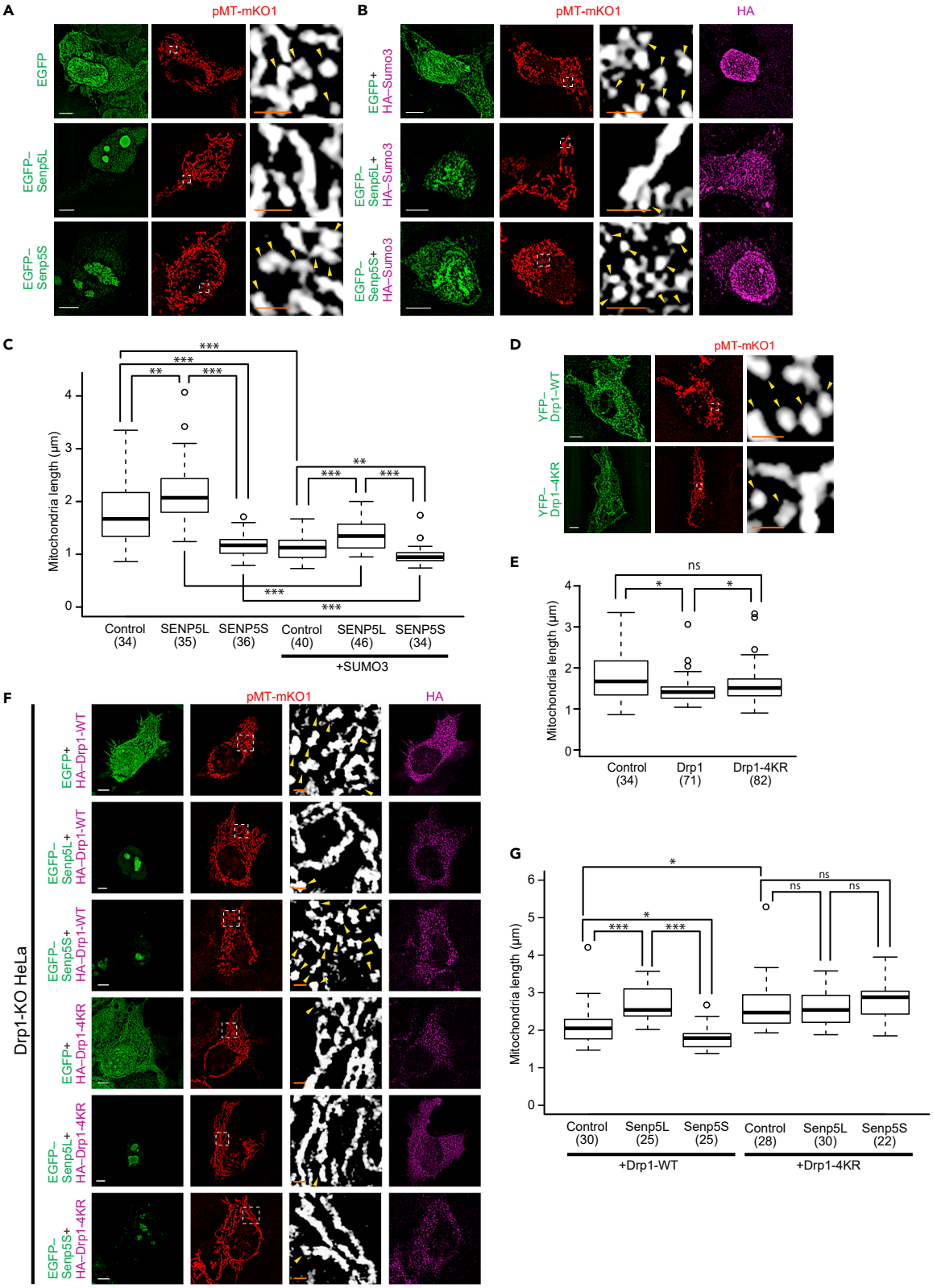
A
pMT-mKO1
EGFP
EGFP–Senp5L
EGFP–Senp5S
B
pMT-mKO1
HA
EGFP+HA–Sumo3
EGFP–Senp5L+HA–Sumo3
EGFP–Senp5S+HA–Sumo3
C
Mitochondria length (μm)
Control (34)
SENP5L (35)
SENP5S (36)
Control (40)
SENP5L (46)
SENP5S (34)
+SUMO3
D
pMT-mKO1
YFP–Drp1–WT
YFP–Drp1–4KR
E
Mitochondria length (μm)
Control (34)
Drp1 (71)
Drp1-4KR (82)
F
Drp1-KO HeLa
pMT-mKO1
HA
EGFP+HA–Drp1-WT
EGFP–Senp5L+HA–Drp1-WT
EGFP–Senp5S+HA–Drp1-WT
EGFP+HA–Drp1-4KR
EGFP–Senp5L+HA–Drp1-4KR
EGFP–Senp5S+HA–Drp1-4KR
G
Mitochondria length (μm)
Control (30)
Senp5L (25)
Senp5S (25)
Control (28)
Senp5L (30)
Senp5S (22)
+Drp1-WT
+Drp1-4KR

Figure 3. Senp5L/5S and Drp1-SUMOylation regulate mitochondrial morphology

(A) Mitochondrial morphologies in 293T cells expressing EGFP, EGFP-Senp5L, or EGFP-Senp5S were analyzed after deconvolution of the confocal projection images. pMT-mKO1 (*red*) was co-transfected to visualize mitochondria. Right column is higher magnification of the boxed areas, depicting individual mitochondrial morphology (*white*). Arrowheads denote fragmented mitochondria.

(B) Overexpression of SUMO3 enhances the mitochondrial fragmentation. Cells were co-transfected with HA-SUMO3 along with EGFP, EGFP-Senp5L, or EGFP-Senp5S. HA-SUMO3 expression was confirmed by immunostaining with anti-HA (*magenta*).

(C) Quantified comparison of the effect of Senp5L, Senp5S, and SUMO3 overexpression on mitochondrial length. Box and whisker plots summarize the length (μm) of mitochondria. Numbers in parentheses indicate the number of cells examined in multiple independent experiments in (A) and (B). **, $p < 0.01$; ***, $p < 0.001$; Welch's t tests with Holm-Bonferroni correction.

(D) Confocal projection images of HEK293T cells transfected with YFP-Drp1-WT or YFP-Drp1-4KR (*green*). pMT-mKO1 (*red*) was co-transfected to visualize mitochondria. Right column: magnified views of the boxed areas showing individual mitochondria (*white*). Arrowheads indicate fragmented mitochondria.

(E) Quantification of mitochondrial length in cells expressing Drp1-WT and Drp1-4KR. Box and whisker plots summarize the mitochondrial length (μm). Numbers in parentheses indicate the number of cells measured for mitochondrial length determination. ns, not significant, *, $p < 0.05$; Welch's t tests with Holm-Bonferroni correction.

(F) Mitochondrial morphologies in Drp1-KO HeLa cells expressing EGFP, EGFP-Senp5L, or EGFP-Senp5S along with HA-Drp1-WT or -4KR were analyzed after deconvolution of the confocal images. HA-Drp1 expression was confirmed by immunostaining with anti-HA (*magenta*). pMT-mKO1 (*red*) was co-transfected to visualize mitochondria. The second column from the right is higher magnification of the boxed areas, depicting individual mitochondrial morphology (*gray scale*). Arrowheads denote the fragmented mitochondria.

(G) Quantified comparison of the effect of EGFP, Senp5L, or Senp5S on mitochondrial length in Drp1-KO HeLa cells expressing either Drp1-WT or Drp1-4KR. Box and whisker plots summarize the length (μm) of mitochondria. Numbers in parentheses indicate the number of cells examined in multiple independent experiments in (F). ns, not significant; *, $p < 0.05$; ***, $p < 0.001$; Welch's t tests with Holm-Bonferroni correction. Scale bars, 5 μm in (A), (B), (D), and (F), and 1 μm in the magnified view.

to be increased by Senp5S (Figure S1A), we did not detect a massive accumulation of SUMOylated proteins compared with the HA-SUMO3-expressing cells (Figure 2A). These results indicated that Senp5S inhibited deSUMOylation, which resulted in the massive accumulation of SUMOylated substrates in cells. Senp5S was likely a competitor against Senp5L.

Senp5 isoforms control Drp1 deSUMO/SUMOylation

It is known that Drp1 SUMOylation by SUMO1 enhances Drp1 stabilization and directs mitochondrial fragmentation (Figueroa-Romero et al., 2009; Guo et al., 2013; Harder et al., 2004) and that SUMO2/3 deconjugation from Drp1 is implicated in cell death (Guo et al., 2013, 2017). However, the role of Senp5 on Drp1 SUMOylation with SUMO3 and mitochondrial dynamics remains elusive. We investigated Drp1 SUMO3-conjugation and the role of Senp5 isoforms. Co-immunoprecipitation (IP) showed SUMO3-ylation of myc-Drp1 and Senp5L-mediated deconjugation, as previously described (Figures 2B and S1C) (Figueroa-Romero et al., 2009). Global SUMO3-ylation was greatly reduced in the cell lysate expressing EGFP-Senp5L. Interestingly, Senp5S clearly enhanced SUMO3-ylation of Drp1 compared with the control (Figure 2B). SUMO3-ylation of Drp1 was confirmed by co-IP using non-SUMOylatable Drp1, in which four acceptor lysine residues encompassing the variable domain were substituted with arginine (Drp1-4KR) (Figueroa-Romero et al., 2009; Guo et al., 2013) (Figure 2C). As shown in Figure 2D, we observed no SUMO3-conjugation with Drp1-4KR. These results showed that Drp1 is a substrate for SUMO3-ylation. Furthermore, Senp5L and Senp5S have opposite effects on Drp1 SUMOylation.

Senp5 isoforms alter mitochondrial dynamics

A previous study reported that overexpression of catalytically active Senp5 in HeLa cells induced mitochondrial elongation (Zunino et al., 2007). Thus, we examined whether Senp5S affected mitochondrial morphology. To visualize the shape of individual mitochondrion, we introduced into HEK293T cells the reporter plasmid mitochondria-targeted monomeric Kusabira-Orange1 (pMT-mKO1) in combination with Senp5L and Senp5S. Consistent with the previous study, Senp5L expression increased mitochondrial length compared with EGFP as a control (Figure 3A). In contrast, Senp5S shortened the mitochondrial length. SUMOylation-dependent fragmentation of mitochondria was further supported by the finding that the overexpression of SUMO3 or SUMO1 caused mitochondrial fragmentation (Figures 3B, S2A, and S2B). SUMO3-induced fragmentation was further increased by Senp5S co-expression and decreased by Senp5L co-expression (Figures 3B and 3C). Although Senp5L and Senp3 inhibited global SUMOylation (Figure 2A), Senp3 shortened rather than elongated mitochondrial length (Figures S2A and S2B), suggesting the involvement of a molecule that is deSUMO/SUMOylated specifically by Senp5L/S, hence contributing to the regulation of mitochondrial dynamics. We then examined the effect of Drp1-SUMOylation on mitochondrial fission by overexpressing Drp1-wild type (WT) or Drp1-4KR. As expected, mitochondrial fragmentation was accelerated by Drp1-WT but not by Drp1-4KR (Figures 3D and 3E). To confirm whether

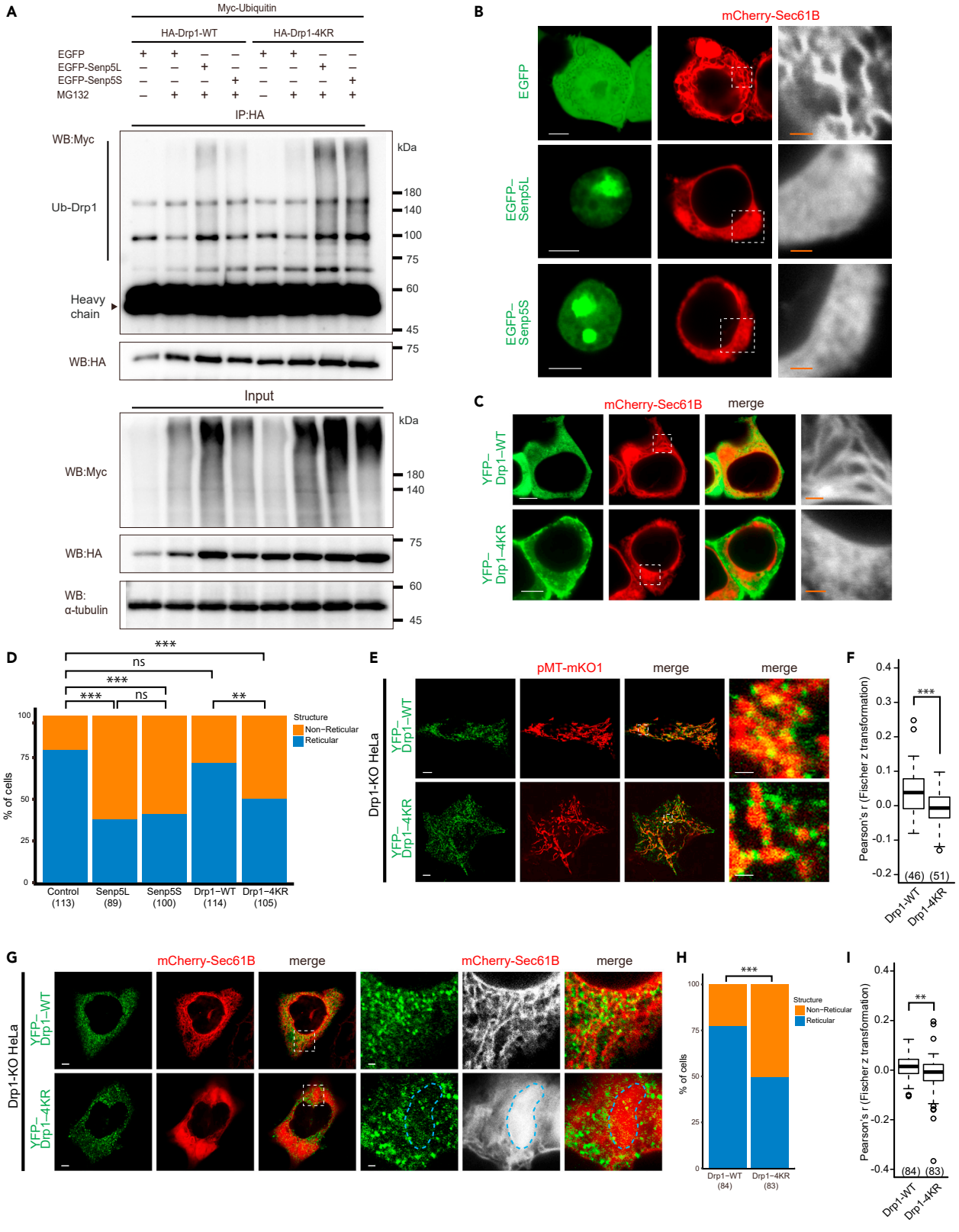
A
Myc-Ubiquitin
HA-Drp1-WT
HA-Drp1-4KR
EGFP
EGFP-Senp5L
EGFP-Senp5S
MG132
IP:HA
WB:Myc
Ub-Drp1
Heavy chain
WB:HA
kDa
180
140
100
75
60
45
Input
WB:Myc
WB:HA
WB: α-tubulin
B
mCherry-Sec61B
EGFP
EGFP–Senp5L
EGFP–Senp5S
C
mCherry-Sec61B
merge
YFP–Drp1–WT
YFP–Drp1–4KR
D
***
ns
***
***
ns
**
% of cells
Structure
Non–Reticular
Reticular
Control (113)
Senp5L (89)
Senp5S (100)
Drp1–WT (114)
Drp1–4KR (105)
E
pMT-mKO1
merge
merge
Drp1-KO HeLa
YFP–Drp1–WT
YFP–Drp1–4KR
F
Pearson's r (Fischer z transformation)
***
(46)
(51)
Drp1-WT
Drp1-4KR
G
mCherry-Sec61B
merge
mCherry-Sec61B
merge
Drp1-KO HeLa
YFP–Drp1–WT
YFP–Drp1–4KR
H
***
% of cells
Structure
Non–Reticular
Reticular
Drp1–WT (84)
Drp1–4KR (83)
I
Pearson's r (Fischer z transformation)
**
(84)
(83)
Drp1-WT
Drp1-4KR

Figure 4. Senp5L/5S are involved in Drp1 ubiquitination and ER dynamics

(A) SUMOylation prevents the ubiquitination of Drp1. HEK293T cells were transfected with Myc-Ubiquitin and HA-Drp1-WT or HA-Drp1-4KR constructs with or without pretreatment with 5 μM MG132 for 3 h. To evaluate the effect of Senp5 on ubiquitination of Drp1, cells were additionally co-transfected with EGFP-Senp5L, EGFP-Senp5S, or (as a control) EGFP. Subsequently, each cell lysate was immunoprecipitated with anti-HA and subjected to immunoblotting with anti-Myc, anti-HA, or anti-α-tubulin. Panels show representative immunoblots for the input lysate (bottom panels) and IP samples (top panels). Drp1 conjugated with Myc-ubiquitin is observed as ladder or smear bands with higher molecular weight (vertical line). Heavy chain, immunoglobulin heavy chain of the HA antibody.

(B) Senp5L and 5S induce morphological change in the ER. 293T cells were transfected with EGFP, EGFP-Senp5L, or EGFP-Senp5S (*green*), together with mCherry-Sec61B (*red*) to monitor the ER network. Right column: higher magnification of the square areas showing mCherry-Sec61B^{+} ER morphology (*gray scale*).

(C) SUMOylation at the D-octadecapeptide of Drp1 is required for inducing tubulation of the ER. HEK293T cells were transfected with mCherry-Sec61B (*red*) and YFP-Drp1-WT or YFP-Drp1-4KR (*green*). Right column: higher magnification of the square areas (*gray scale*).

(D) Quantified comparison of the effect of Senp5L, Senp5S, or Drp1-4KR overexpression on ER morphology. The stacked bar chart shows the percentages of cells that exhibit a tubulated reticular ER or a sheet-like, non-reticular ER. Numbers in parentheses indicate the number of cells observed in two independent experiments in (B) and (C). ns, not significant; **, $p < 0.01$; ***, $p < 0.001$; chi-square tests with Holm-Bonferroni correction.

(E) Drp1 SUMOylation alters co-localization with mitochondria. Drp1-KO HeLa cells were transfected with pMT-mKO1 (*red*) and YFP-Drp1-WT or YFP-Drp1-4KR (*green*). Right column, higher magnification of the boxed areas.

(F) Quantified comparison of the co-localization of YFP-Drp1-WT or YFP-Drp1-4KR with mitochondria. Fischer z-transformation of Pearson's correlation coefficient was used as a co-localization index and summarized in box and whisker plots. ***, $p < 0.001$; Welch's t test.

(G) Drp1 SUMOylation alters co-localization with ER. Drp1-KO HeLa cells were transfected with mCherry-Sec61B (*red*) and YFP-Drp1-WT or YFP-Drp1-4KR (*green*). Right columns, higher magnification of the boxed areas. Hatched region in panels denote the non-reticular ER.

(H) Quantification of the effect of YFP- Drp1-WT or Drp1-4KR overexpression in Drp1-KO HeLa cells on ER structure. The stacked bar chart shows the percentages of cells that exhibit a tubulated reticular ER or a sheet-like, non-reticular ER. Numbers in parentheses indicate the number of cells observed in three independent experiments. ***, $p < 0.001$; chi-square test.

(I) Quantified comparison of the co-localization YFP-Drp1-WT or YFP-Drp1-4KR with ER. Fischer z-transformation of Pearson's correlation coefficient was used as a co-localization index and summarized in box and whisker plots. Numbers in parentheses indicate the number of cells observed in three independent experiments. **, $p < 0.01$; Welch's t tests. Scale bars, 5 μm in (B), (C), (E), and (G) and 1 μm in the magnified view.

Senp5L/S regulates mitochondrial dynamics through SUMOylation of Drp1, we used Drp1-KO HeLa cells (Saita et al., 2016). Consistent with the previous study (Saita et al., 2016), the mitochondrial length was significantly longer in Drp1-KO cells than in wild-type HeLa cells (Figures S2C and S2D). In the presence of exogenously expressed Drp1-WT, Senp5L and Senp5S elongated and shortened mitochondria, respectively, in Drp1-KO cells (Figures 3F and 3G). These Senp5L/S-dependent changes in mitochondrial length were totally abolished in the Drp1-4KR background (Figures 3F and 3G). We concluded that Senp5L and Senp5S promote mitochondrial fusion and fission, respectively, *via* the regulation of Drp1 deSUMO/SUMOylation. Considering the competitive nature of Senp5 isoforms, the expression levels of Senp5L and Senp5S might be critical for mitochondrial dynamics.

Senp5 isoforms alter Drp1 ubiquitination and endoplasmic reticulum morphology

Although the molecular mechanism of Drp1 modulation by SUMO3 remained unclear, one plausible explanation was that Drp1 conjugation with SUMO3 prevented ubiquitination, thus inhibiting the proteasome-mediated degradation of Drp1 (Harder et al., 2004). We examined Drp1 ubiquitination in the presence of exogenous Senp5L or Senp5S and found an increased level of ubiquitinated Drp1 in cells expressing Senp5L with or without treatment with N-ethyl-maleimide, a cysteine peptidases inhibitor (Figure S3A). To further test whether Drp1 ubiquitination was dependent on SUMOylation, we analyzed the ubiquitination level of Drp1-WT and Drp1-4KR. Cells were transfected with myc-ubiquitin together with HA-Drp1-WT or -4KR, and EGFP-Senp5L or -Senp5S. The extracts were immunoprecipitated with anti-HA antibody, then the ubiquitinated Drp1-WT and -4KR were determined. Drp1-4KR was more ubiquitinated than Drp1-WT when pretreated with MG132, a proteasome inhibitor (Figures 4A and S3B). Noticeably, Drp1-WT ubiquitination was increased when co-expressed with Senp5L. We also found less ubiquitination of Drp1-WT in Senp5S compared with Senp5L-expressing cells. Furthermore, ubiquitination level of Drp1-4KR was high regardless of cells expressed Senp5L or 5S. These results indicated that deSUMOylation catalyzed by Senp5L promoted Drp1 ubiquitination, which could lead to decreased Drp1 activity and thus mitochondrial elongation. These findings were consistent with our results on mitochondrial length (Figure 3), except that the ubiquitination level of Drp1-4KR + EGFP was lower than those of +Senp5L and 5S.

Another possible explanation for the involvement of Senp5 in mitochondrial dynamics was an influence of Senp5 on Drp1-dependent regulation of endoplasmic reticulum (ER) structure. A recent study reported that four lysine residues in the variable domain of Drp1 play a critical role in ER tubulation and

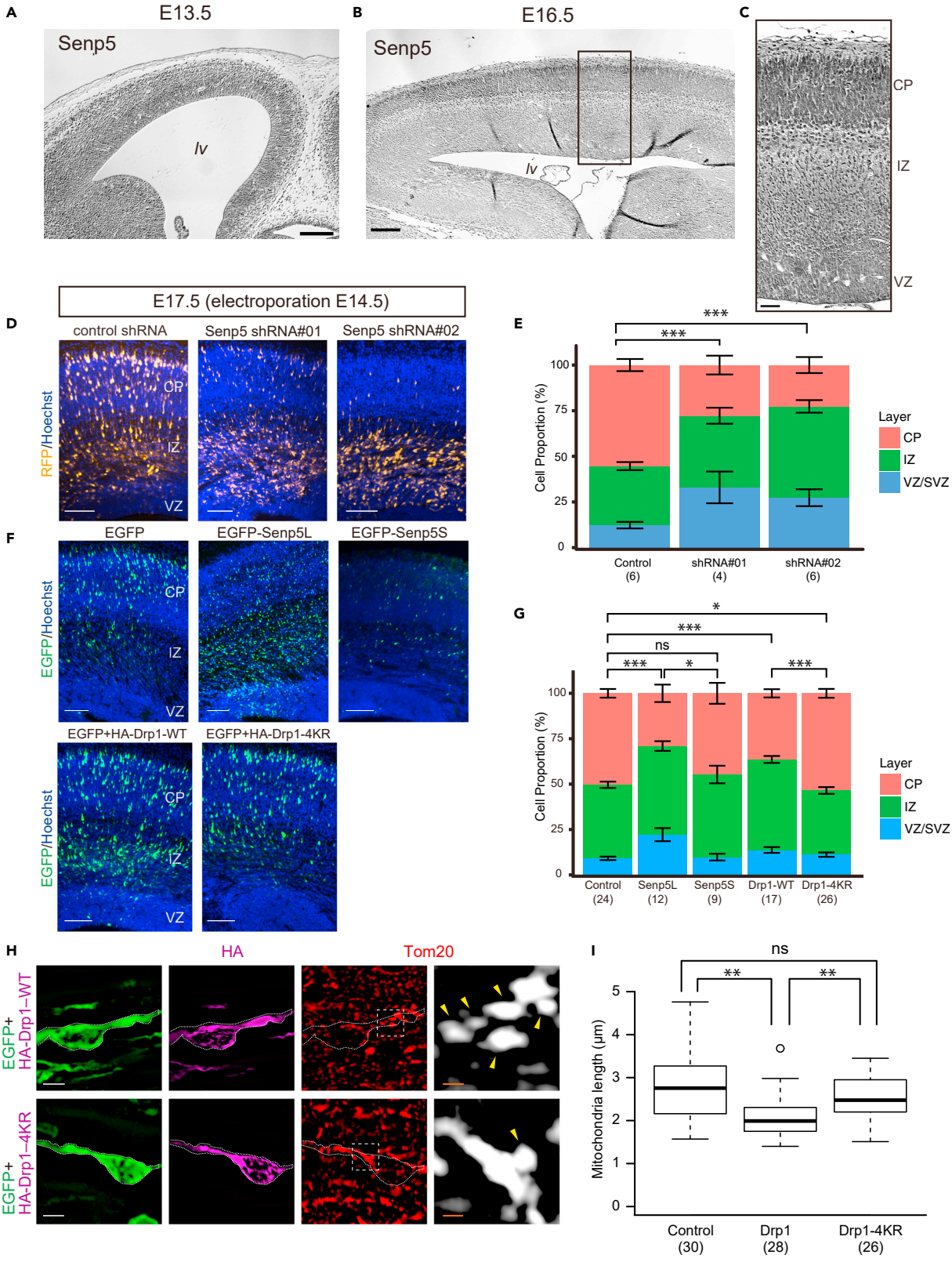
A
E13.5
Senp5
lv
B
E16.5
Senp5
lv
C
CP
IZ
VZ
D
E17.5 (electroporation E14.5)
control shRNA
Senp5 shRNA#01
Senp5 shRNA#02
RFP/Hoechst
CP
IZ
VZ
E
***
***
Cell Proportion (%)
100
75
50
25
0
Control
(6)
shRNA#01
(4)
shRNA#02
(6)
Layer
CP
IZ
VZ/SVZ
F
EGFP
EGFP-Senp5L
EGFP-Senp5S
EGFP/Hoechst
CP
IZ
VZ
EGFP+HA-Drp1-WT
EGFP+HA-Drp1-4KR
G
*
***
ns
***
*
***
Cell Proportion (%)
Control
(24)
Senp5L
(12)
Senp5S
(9)
Drp1-WT
(17)
Drp1-4KR
(26)
Layer
CP
IZ
VZ/SVZ
H
HA
Tom20
EGFP+
HA-Drp1–WT
EGFP+
HA-Drp1–4KR
I
ns
**
**
Mitochondria length (μm)
5
4
3
2
1
0
Control
(30)
Drp1
(28)
Drp1-4KR
(26)

Figure 5. Dysregulation of Senp5L/5S expression or Drp1-SUMOylation causes migration defects of neurons in embryonic cerebral cortex

(A–C) Distribution of Senp5 in embryonic cortex. Coronal sections of cerebral cortex at E13.5 (A) and E16.5 (B) were immunostained with anti-pan-Senp5 antibody. (C) Higher magnification of the boxed area of (B). lv, lateral ventricle; CP, cortical plate; IZ, intermediate zone; VZ, ventricular zone.

(D and E) Senp5 knockdown (KD) induces accumulation of migrating neurons in the IZ. Non-targeting control shRNA or Senp5 shRNA construct (shRNA #01 or shRNA #02) was electroporated into E14.5 cortices *in utero* together with TurboRFP. (D) Coronal sections of E17.5 cortex showing the distribution of TurboRFP$^+$ cells expressing shRNA (*yellow*). Nuclei were counterstained with Hoechst dye (*blue*). (E) Distribution of TurboRFP$^+$ cells in the indicated areas at E17.5. ***, $p < 0.001$; two-way ANOVA with Holm-Bonferroni correction.

(F and G) Overexpression of Senp5L or Drp1-WT represses neuronal migration. (F) EGFP-Senp5L, EGFP-Senp5S, HA-Drp1-WT (with EGFP), HA-Drp1-4KR (with EGFP), or control EGFP (*green*) was electroporated *in utero* at E14.5, and the neocortex was analyzed at E17.5. (G) Distribution of electroporated EGFP$^+$ cells in the indicated areas. ns, not significant; *, $p < 0.05$; ***, $p < 0.001$; two-way ANOVA with Holm-Bonferroni correction. Numbers in parentheses indicate the number of embryos analyzed.

(H) Magnified view of immature neurons migrating in the IZ of the brain electroporated with HA-Drp1-WT or HA-Drp1-4RK. Sections were immunostained with anti-Tom20 (*red*) and anti-HA (*magenta*). Right: Higher magnification of the boxed areas showing the morphology of Tom20$^+$ mitochondria (*white*). Arrows denote fragmented mitochondria.

(I) Box and whisker plots summarize the mitochondrial length data (μm). Forced expression of Drp1-WT altered mitochondrial morphology in migrating neurons. Numbers in parentheses indicate the number of cells analyzed. ns, not significant; **, $p < 0.01$; Welch's t tests with Holm-Bonferroni correction. Stacked bar charts represent mean ± SEM. Scale bars: 100 μm in (A) and (B), 25 μm in (C), 100 μm in (D) and (F), 5 μm in (H), and 1 μm in the magnified view.

mitochondrial fragmentation (Adachi et al., 2020). These four lysine residues are identical to the SUMOylation sites (K557, K560, K569, and K571) (Figure 2C). Thus, we hypothesized that Drp1 SUMO/de-SUMOylation regulates ER tubulation. To test this idea, we examined the ER architecture in HEK293T cells expressing Senp5L or Senp5S. ER membranes were visualized using ER-resident mCherry-Sec61B. As shown in Figure 4B, tubulated and reticular ER were observed in EGFP-control cells, whereas exogenous expression of Senp5L or Senp5S significantly decreased reticular ER. To test the involvement of Drp1 SUMOylation in ER tubulation, Drp1-WT or the Drp1-4KR construct was introduced into HEK293T cells. Drp1-4KR but not Drp1-WT disrupted the reticular ER structure (Figures 4C and 4D). We next examined localization of Drp1-WT and Drp1-4KR to mitochondria and ER using Drp1 KO HeLa cells (Figures 4E–4I). Drp1-WT showed significantly higher co-localization with mitochondria than that of Drp1-4KR (Figures 4E and 4F). Furthermore, Drp1 co-localization on ER was also higher in Drp1-WT than in Drp1-4KR (Figure 4I). This may be explained by the effect of Drp1-4KR on ER structure: Drp1-4KR increased the population of cells exhibiting non-reticular and sheet-like ER (Figure 4H), and Drp1 signals were barely detectable in the area with de-structured ER (Figure 4G, hatched area), leading to decrease in the ER co-localization. Consistently, previous study reported the decreases in ER tubules along with the mitochondrial elongation in Drp1-KO cells (Adachi et al., 2020). These observations support the conjecture that SUMOylated Drp1 molecules elicit ER tubulation, ensuing mitochondrial fragmentation. Suppression of ER tubulation by Senp5S implies importance of stringent control of deSUMO/SUMOylation by Senp5L and Senp5S in Drp1-mediated ER tubulation and/or an existence of effector molecule(s), which regulates ER tubulation in a Drp1-independent manner, downstream of Senp5L/5S.

Senp5 expression during the brain neurogenesis

To explore the *in vivo* function of the Senp5 isoforms, we examined the Senp5 expression profile in embryonic cerebral cortices at different stages of neurogenesis and the ensuing cell differentiation. Senp5 antibody used in this study can recognize both Senp5L and S proteins. At E13.5, Senp5 immunoreactivity was observed throughout the neocortex including the ventricular zone (VZ) surrounding the lateral ventricles, where many NSPCs undergo cell division to generate immature neurons (Figure 5A). Later, at E16.5, dense Senp5 immunoreactivity was observed in the CP, while a substantial level of expression continued in the VZ, SVZ, and intermediate zone (IZ) (Figures 5B and 5C). These immunohistochemical data showed persistent Senp5 expression in neuronal lineage. The expression profile of Senp5 was comparable with that of Senp3 in the developing cortex (Figures S4A–S4C).

Senp5 in cerebral cortex development

To gain direct insight into the role of Senp5 isoforms in brain development, we performed *in vivo* knockdown (KD) and overexpression experiments, using *in utero* electroporation in mouse embryos. Plasmids encoding the short hairpin RNA (shRNA) and turboRFP were delivered by electroporation into NSPCs in E14.5 embryos through the lateral ventricle, and the brain sections were prepared 3 days later (E17.5). Owing to the technical difficulty of designing effective shRNAs specific to Senp5S, we used shRNA constructs (shRNA#01 and #02) that knocked down both Senp5L and 5S (Figure S5) (Akiyama et al., 2018). In control embryos electroporated with scrambled shRNA, new-born turboRFP$^+$ neurons radially migrated

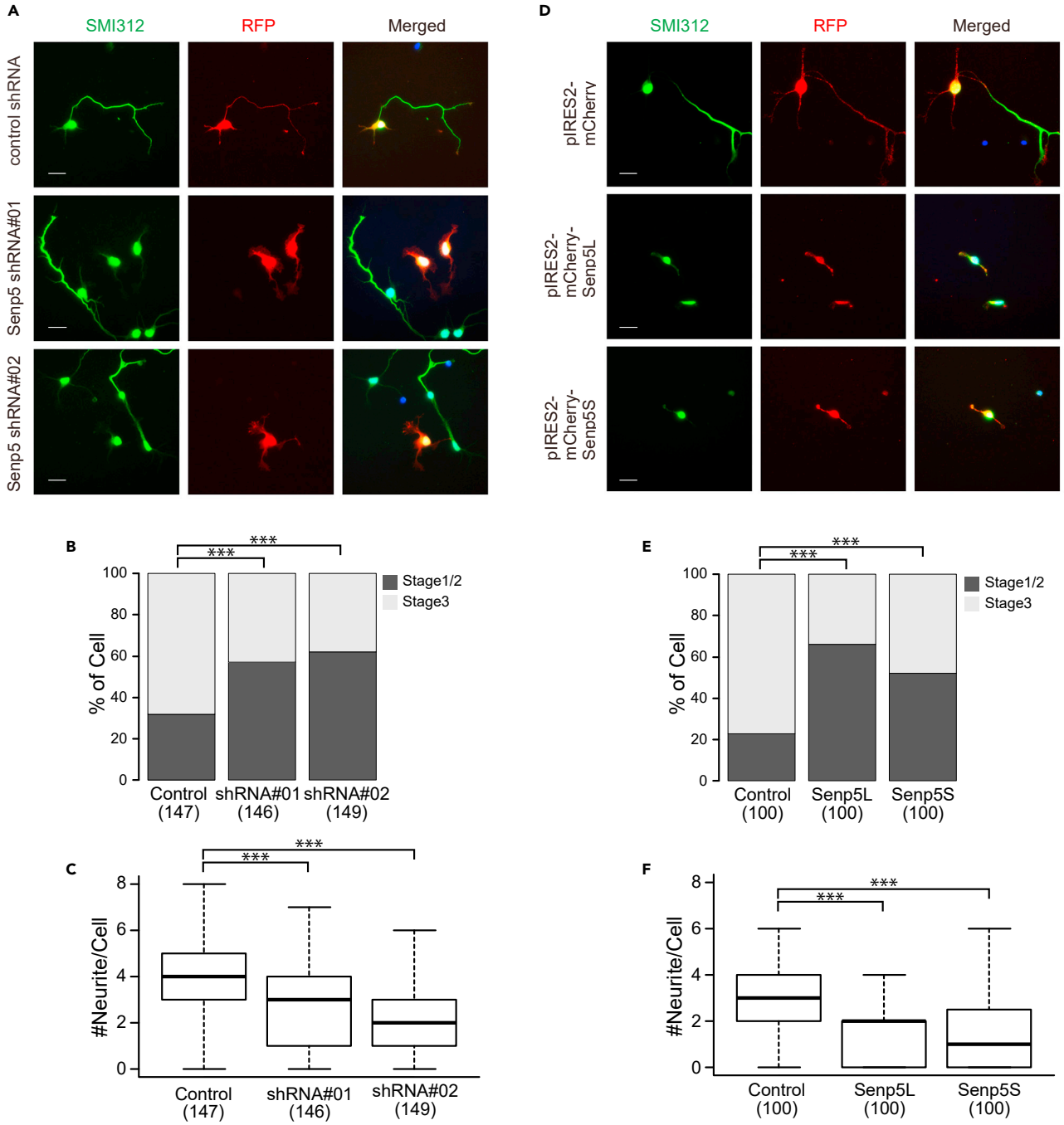

Figure 6. Senp5L/5S regulate neurite outgrowth and polarization

(A–C) Senp5 shRNAs (shRNA #01 or shRNA #02) or control shRNA was introduced into primary cultured cortical neurons along with a reporter plasmid encoding red fluorescent protein (RFP) (*red*). (A) Neurofilaments in individual neurons were stained with anti-SMI312 (*green*) at 3 div. (B) The stacked bar chart shows the percentages of cells having SMI312$^+$ axons (stage 3). Numbers in parentheses indicate the number of cells analyzed. ***, $p < 0.001$; chi-square tests with Holm-Bonferroni correction. (C) Box and whisker plots summarize the numbers of RFP$^+$ neurites extending from individual neurons. Numbers in parentheses indicate the number of cells measured in three independent experiments. ns, not significant; ***, $p < 0.001$; Wilcoxon rank sum tests with Holm-Bonferroni correction.

(D–F) Overexpression of Senp5L and Senp5S in immature neurons. pIRES2-mCherry-Senp5L, pIRES2-mCherry-Senp5S, or control pIRES2-mCherry was electroporated into primary cultured cortical neurons. Neurofilaments and mCherry were stained with anti-SMI312 (*green*) and anti-RFP (*red*) at 3 div. (E) The

Figure 6. *Continued*
stacked bar chart shows the percentages of cells having SMI312$^+$ axons (stage 3). Numbers in parentheses indicate the number of cells measured in three independent experiments; ***, $p < 0.001$; chi-square tests with Holm-Bonferroni correction. (F) Box and whisker plots summarize the numbers of RFP$^+$ neurites extending from individual neurons. Numbers in parentheses indicate the number of cells measured. ns, not significant; ***, $p < 0.001$; Wilcoxon rank sum tests with Holm-Bonferroni correction. Scale bars, 20 μm.

away from the VZ toward the pial surface. Numerous turboRFP$^+$ cells reached the CP (Figure 5D). By contrast, Senp5 KD hindered cell migration into the CP (% of cells in CP: control, 55.4 ± 3.3%, n = 6; SENP5 shRNA #01, 27.8 ± 5.2%, n = 4; SENP5 shRNA #02, 22.6 ± 4.4%, n = 6; Figure 5E), resulting in statistically significant difference in the proportion of cells positioned in each layer. These results indicated a critical role for Senp5 in neuronal migration and corticogenesis.

Next, we assessed the overexpression phenotype of each Senp5 isoform. As shown in Figures 5F and 5G, EGFP-Senp5L significantly inhibited neuronal migration into the CP (% of cells in CP: EGFP, 50.4 ± 2.9%, n = 24; Senp5L; 29.0 ± 4.8%, n = 12). However, the embryos electroporated with EGFP-Senp5S did not exhibit any deranged cortical organization or impaired neuronal migration (% of cells in CP: 44.7 ± 5.7%, n = 9; Figure 5G). Notably, the number of EGFP-Senp5S$^+$ cells in specimens was extremely low (Figure 5F) compared with that of Senp5L or control EGFP. Although the reason for this lower level of expression is unclear, translational suppression or developmental control on Senp5S mRNA might be involved. Considering the phenotypic equivalence between KD and overexpression of Senp5L, we conclude that a strictly controlled level of Senp5L expression must be required for cortical development.

Drp1 SUMOylation status regulation appropriate for the cortical development

To examine whether Drp1 SUMOylation status influenced the brain development, HA-Drp1-WT or HA-Drp1-4KR was electroporated *in utero* into E14.5 brains and the brains were analyzed at E17.5. As shown in Figure 5F, overexpression of Drp1-WT suppressed neuronal migration into CP (% of cells in CP: 36.4 ± 2.3%, n = 17). However, Drp1-4KR only showed modest defects in cortical organization (CP: 53.5 ± 2.4%, n = 26) compared with control (Figures 5F and 5G). These results showed that aberrant cortical development caused by Drp1-WT was dependent on the SUMOylation of Drp1. We further investigated whether Drp1 SUMOylation affected mitochondrial dynamics by anti-Tom20 immunostaining of neurons in the IZ that were extending the leading process and acquiring polarization. Consistent with the results obtained with HEK293T cells (Figures 3D and 3E), Drp1-WT overexpression shortened the average mitochondrial length of migrating neurons, whereas Drp1-4KR expression abolished this fragmentation phenotype (Figures 5H and 5I). Dysregulated expression of Senp5 by KD and overexpression probably leads to inappropriate Drp1-SUMOylation. Under such conditions, tight control over mitochondrial fission/fusion would be lost, which would result in impaired motility of immature neurons.

Senp5 isoforms regulate neuronal polarization

Neuronal polarization can occur simultaneously with cortical neuronal migration (Hansen et al., 2017). To elucidate whether Senp5 isoforms are involved in polarity formation in migrating neurons, we performed Senp5 overexpression and KD experiments using a culture of dissociated cortical neurons prepared from E16-17 embryos. TurboRFP or mCherry was used to visualize processes extending from individual neurons. Anti-SMI312 immunostaining was performed to detect axon formation. By 3 div, most cells transfected with non-targeting control shRNA had established polarity (stage 3; Figure 6A). In contrast, more than half of the neurons with reduced Senp5 levels remained in unpolarized stages (stage 1/2; Figures 6A and 6B). Furthermore, Senp5 KD cells extended a significantly small number of neurites compared with the control cells (Figure 6C). To assess the role of the Senp5 isoforms individually, cortical neurons were transfected with Senp5L or 5S. Expression of exogenous Senp5L and Senp5S caused defects in the acquisition of neuronal polarity (Figures 6D and 6E). Furthermore, the number of neurites was significantly less in Senp5L- and Senp5S-expressing neurons than in control neurons (Figure 6F). These results demonstrated the essential role of Senp5 isoforms in neuronal polarization. Since all experimental conditions, including KD and Senp5 isoform overexpression, elicited similar defects in neurons, the balanced expression of Senp5L and Senp5S appears to be a requirement for neurite outgrowth and polarity formation, and thus for proper corticogenesis.

DISCUSSION

Members of the Senp family (Senp1-8) share a conserved C-terminal catalytic domain that subserves their cysteine protease activities, whereas their N-terminal regions have diverse specific functions (Kunz et al.,

2018). All identified Senps have isopeptidase activity, which mediates the deSUMOylation of target proteins. In addition, several Senps have endopeptidase activity, which converts pro-SUMO into conjugatable mature SUMO capable of SUMOylation. Conventional Senps can control both SUMOylation and deSUMOylation depending on protease activity. We revealed a novel protease-independent mechanism for SUMO cycle regulation, in which the newly identified Senp5S, which lacks protease activity, promoted SUMOylation by competing with other Senps for the regulation of SUMOylation status (Figure 7A).

Like Senp5S, several catalytically inactive splice variants are known to regulate post-translational modification. FAK-related and PYK2-related non-kinase inhibit phosphorylation mediated by FAK and PYK2, respectively (Parsons, 2003). Another example is protein-tyrosine phosphatase 1B (PTP1B). The variant of PTP1B lacking a catalytic center promotes phosphorylation by competing with PTP1B to maintain tumor cell survival and proliferation (Zahn et al., 2021). In addition, a catalytically inactive form of TRE/ubiquitin specific protease (UPS6) has been identified, although it remains unclear whether the short isoform and the full-length USP6 competitively regulate the ubiquitination of target proteins (Madan et al., 2016; Shen et al., 2005). These findings support competitive regulation by catalytically active and inactive splice variants as a common strategy for tuning the post-translational modification state of the target molecule. In the present study, we demonstrated the physiologically crucial role of this mechanism, in which Senp5 isoforms had an opposite activity on Drp1 modification and competitively regulated mitochondrial dynamics, thus allowing tight control of neuronal differentiation and corticogenesis.

We showed that Senp5L and Senp5S had opposite effects on SUMO conjugation to Drp1. Senp5L promoted deSUMOylation, whereas Senp5S facilitated SUMOylation. SUMO deconjugation from/conjugation to Drp1 mediated by each isoform, respectively, caused mitochondrial elongation/fragmentation (Figure 7B). Several studies have implicated Drp1 SUMOylation in the regulation of mitochondrial dynamics. SUMOylated Drp1 confines to mitochondrial fission site (Harder et al., 2004), and the variable domain containing four SUMOylation sites is required for Drp1 localization to mitochondria (Fröhlich et al., 2013; Guo et al., 2017). SUMOylation-induced mitochondrial fragmentation was rescued by overexpression of Senp5L, partly owing to the downregulation of Drp1 (Zunino et al., 2007). The interaction between mitochondria and the ER is shown to be involved in mitochondrial dynamics. SUMOylated Drp1 functionally stabilizes ER-mitochondrial interacting sites for constriction (Prudent et al., 2015). Furthermore, the variable domain is required for mitochondrial fission and ER tubulation (Adachi et al., 2020). Aligning with these evidences, we examined two possible, non-mutually exclusive, mechanisms for Senp5-dependent control of mitochondrial dynamics. One was through Drp1 ubiquitination, whereas the other was through Drp1 localization and ER tubulation. Previous studies suggested that Drp1 was stabilized by SUMO1-conjugation and SUMO1-ylated Drp1 promoted mitochondrial fragmentation (Harder et al., 2004). This allowed us to speculate that deSUMOylated Drp1 is a labile form, the formation of which might be quickly followed by protein degradation. Indeed, we showed that Senp5L overexpression enhanced the ubiquitination of Drp1, which led to a lower rate of mitochondrial fission in Senp5L expressing cells. In contrast, Senp5S is likely to stabilize Drp1 by promoting SUMOylation, resulting in mitochondrial fragmentation (Figure 7B). Our results on ubiquitination of Drp1 showed that, although high level of ubiquitination was observed in Senp5L, Senp5S also increased Drp1 ubiquitination compared with control, suggesting the involvement of mechanism(s) other than Drp1 stabilization in Senp5-mediated control of mitochondrial dynamics.

Drp1 distributed around the ER induces ER tubulation independent of its GTPase activity. This structural change facilitated contacts between the ER and mitochondria, leading to mitochondrial fragmentation (Adachi et al., 2020). Binding between Drp1 and phosphatidic acid (PA) played an essential role in Drp1-mediated ER tubulation, which required four lysines in the D-octadecapeptide sequence (Adachi et al., 2020). Here, we used Drp1-4KR to demonstrate ER de-structuration, consistently showing the involvement of the four lysines in ER tubulation. Since arginine was used to substitute for lysine rather than alanine, it was unclear whether PA binding was inhibited in our experimental condition. Drp1-4KR would have retained the binding ability if it bound to PA electrostatically. How does SUMOylation regulate the ER tubulation and mitochondrial dynamics? One possible scenario is that Senp5 isoforms control the intracellular distribution of the Drp1 pool as the regulator of SUMOylation level of Drp1. Our finding of decreased co-localization of Drp1-4KR to the mitochondria and ER supports this idea. Consistently, the variable domain of Drp1 was necessary for the recruitment of Drp1 to the mitochondria (Fröhlich et al., 2013; Guo et al., 2017), suggesting the involvement of SUMOylation in the intracellular trafficking of Drp1. Drp1 exists in the cytosol as a pool of dimers and tetramers and is recruited by the Drp1 receptors Mff

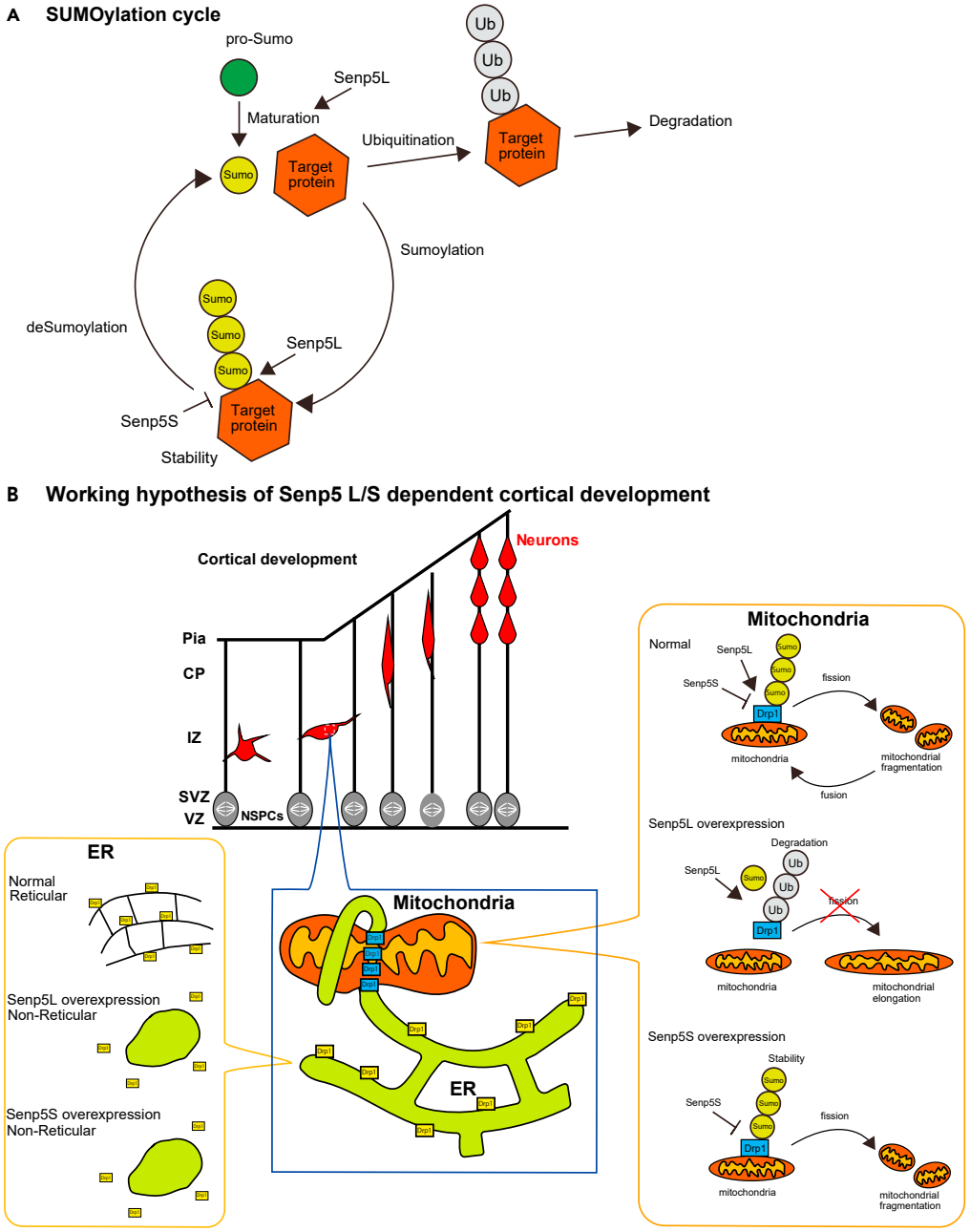

Figure 7. Schematic model of how Senp5L and Senp5S mediate Drp1 SUMOylation

(A) Shown is the SUMOylation cycle and the roles of Senp5L/5S. Senp5L removes SUMO from the target proteins (deSUMOylation) and Senp5S promotes SUMOylation, probably by substrate competition with other Senps, including Senp5L. Senp5L also is known to cleave pro-SUMO to produce the mature and conjugatable form of SUMO.

(B) Hypothetical function of Senp5L/S in regulating cortical development. A tuned balance between Senp5L and Senp5S expression is indispensable for neuronal polarization and cortical organization. Overexpression of Senp5L accelerates deSUMOylation and ubiquitination of Drp1, and thus mitochondrial fusion. Senp5L overexpression also induces the morphological transformation of ER into the non-reticular form, which reduces the availability of interface sites between the peripheral ER and mitochondria, further promoting mitochondrial elongation. However, overexpression of Senp5S enhances Drp1-SUMOylation, resulting in the stabilization of Drp1 and mitochondrial fragmentation. Enhanced SUMOylation due to Senp5S upregulation may lead to disruption of the interaction between the ER and mitochondria and a subsequent collapse of the reticular ER.

or MiD51/MiD49 located on the mitochondrial membrane to produce mitochondrial constriction. MiD51/MiD49 may recruit the Drp1 dimer, whereas Mff may selectively bond to the higher-order Drp1 complexes (Liu and Chan, 2015), suggesting the existence of Drp1-assembling machinery. In this context, deSUMO/SUMOylation mediated by Senp5L/5S functioned to affect the conformational change and assembly of Drp1 protein, resulting in the recruitment of subpopulations of Drp1 from the cytosol to the mitochondrial fission site. Further study is needed to unveil the precise mechanism of Senp5L/S-dependent control of mitochondrial dynamics.

Senp5 is involved in various cellular aspects including mitosis, differentiation, and apoptosis in HeLa cells or hiPS-cardiomyocytes (Kim et al., 2015; Zhang et al., 2020; Zunino et al., 2009); however, its physiological significance in the brain is unknown. We demonstrated the involvement of Senp5 isoforms in corticogenesis, to some extent, by regulating neurite outgrowth and/or neuronal polarization. Given that both knockdown and overexpression of Senp5L and Senp5S impaired neuronal development, tightly controlled expression balance between the two isoforms is presumed to be important. Mitochondrial fragmentation impairs neurite outgrowth from cortical neurons in culture, and Drp1, which targets mitochondria, seems to play crucial roles (Zhao et al., 2019). One can speculate that Senp5 isoforms exert their effects through SUMOylation/deSUMOylation-dependent targeting of Drp1 to mitochondria. In our examinations of cortical development, Senp5L overexpression inhibited the migration of cortical neurons, whereas Drp1-4KR had little effect on migration. This apparent discrepancy may be explained by background Drp1 activity remaining in Drp1-4KR expressing neurons. We also showed that Senp5 isoforms disturbed neuronal polarization. Although it is unclear whether the defects in polarity formation are a result of impaired neurite outgrowth, axon specification can be controlled by mitochondrial dynamics (Ruthel and Hollenbeck, 2003) and thus by Senp5 isoforms.

There is another possible explanation as to how Senp5 isoforms regulate corticogenesis (Ishihara et al., 2009; Iwata et al., 2020). Recent *in vivo* imaging studies using mouse embryonic forebrain revealed that NSPCs have an increased ability to undergo mitochondrial fusion, whereas some daughter cells that acquire a high level of mitochondrial fission are destined to be neurons (Iwata et al., 2020). Therefore, neuronal differentiation can be regulated by mitochondrial dynamics. Considering the expression of Senp5 isoforms in the neuronal lineage from the early to late stage of the brain development, Senp5 may be involved in broad aspects of neurogenesis that are closely linked with Drp1 and consequent mitochondrial dynamics.

The expression levels of the Senp5 isoforms in the brain changed as development proceeded; Senp5S expression was drastically upregulated in postnatal and adult brains. Our previous immunoelectron microscopy study revealed that, in the adult brain, Senp5 protein localizes to presynaptic terminals, postsynaptic spines, and mitochondria (Akiyama et al., 2018), suggesting a functional relevance of Senp5S to synaptogenesis and synaptic transmission in the mature neuron. Since we confirmed the expression of the Senp5S isoform in humans (UniProt number; Q96HI0-2), which lacks His-646 and Asp-663 in the C-terminal catalytic triad (Hickey et al., 2012), it is likely that Senp5S plays an evolutionarily conserved role in the development and maintenance of the mammalian nervous system. SUMOylation promotes the stability of several target proteins by antagonizing their ubiquitination (Bellail et al., 2014; Harder et al., 2004; Rott et al., 2017; Wen et al., 2017). An imbalance between SUMOylation and deSUMOylation is implicated in various neurodegenerative diseases in humans such as Alzheimer's disease (AD), amyotrophic lateral sclerosis (ALS), Parkinson's disease (PD), and developmental abnormalities (Schaffert and Carter, 2020). In AD, the enhanced SUMOylation of tau was detected in cerebral cortex. SUMOylation inhibited ubiquitination-mediated tau degradation, leading to the accumulation of insoluble aggregates of tau in the AD brain (Luo et al., 2014). Similarly, SUMOylation is involved in SOD1 aggregation in ALS and α-Synuclein aggregation in PD (Niikura et al., 2014; Rott et al., 2017). In addition, several genes associated with PD, such as α-Synuclein, Pink1, and Parkin, control mitochondrial function and morphology. If Senp5L and 5S function in the SUMOylation of these proteins in the adult brain, Senp5 would be a possible therapeutic target for degenerative disorders.

Limitations of the study

The present study had some limitations. First, we mainly used tag-conjugated SUMO3 to demonstrate Senp5 L/S-dependent control of Drp1 SUMOylation status. Given that Drp1-4KR is not able to be SUMOylated with SUMO3 as well as SUMO1 and that Senp5L/S inhibits/promotes global SUMO1-ylation, not only SUMO3 but also SUMO1 is possibly involved in Senp5 L/S-dependent control of Drp1 SUMOylation and mitochondrial dynamics. Second, we demonstrated crucial roles of Senp5L/S in the regulation of mitochondrial dynamics and corticogenesis with a genetical approach including isoform-specific gain-of-function.

Nevertheless, sh/siRNA for isoform-specific loss of function and antibodies that separately recognize each isoform would advance our understanding on physiological significance of Senp5 isoforms.

STAR★METHODS

Detailed methods are provided in the online version of this paper and include the following:

- KEY RESOURCES TABLE
- RESOURCE AVAILABILITY
  - Lead contact
  - Materials availability
  - Data and code availability
- EXPERIMENTAL MODEL AND SUBJECT DETAILS
  - Mice
- METHOD DETAILS
  - Cell culture and transfection
  - Cloning of mouse Senp5 cDNAs
  - Quantitative PCR
  - Plasmids
  - *In utero* electroporation
  - Immunoprecipitation and immunoblotting
  - Immunocytochemistry
  - Immunohistochemistry
  - Analysis of mitochondrial and ER morphology
  - Analysis of co-localization
- QUANTIFICATION AND STATISTICAL ANALYSIS
  - Statistical analysis

SUPPLEMENTAL INFORMATION

Supplemental information can be found online at https://doi.org/10.1016/j.isci.2021.103484.

ACKNOWLEDGMENTS

The authors would like to thank Dr. C. Guo (The University of Sheffield, UK) for sharing the YFP-Drp1-WT and YFP-Drp1-4KR plasmid, Dr. M. Kengaku for the myc-Drp1, and Dr. T. Nishida (Mie University, Japan) for the EGFP-Senp3 and EGFP-Senp5L. We would like to thank Editage (www.editage.com) for English language editing. We would also thank Mrs. Y. Ishiguro and D. Yasui (Waseda University) for technical assistance.

This work was funded by the Japan Society for the Promotion of Science grants-in-aid [KAKENHI] grant numbers 18K06491 (to H.A.) and 26430042 (to S.S.) and by Waseda University Grants for Special Research Projects 2018K-352 (to H.A.), 2015K-249, and 2017K-301 (to S.S.).

AUTHOR CONTRIBUTIONS

All authors have full access to the data of this study and take responsibility for its integrity and accuracy. Study concept and design: S.Y., H.A., and S.S. Acquisition of data: S.Y., A.S., H.A., and S.S. Preparation of experimental materials: S.Y., A.S., H.A., N.I., and S.S. Analysis and interpretation of data: S.Y., A.S., H.A., and S.S. Drafting of the manuscript: S.Y., H.A., and S.S. Critical revision of the manuscript: H.A., N.I., and S.S. Obtained funding: H.A. and S.S.

DECLARATION OF INTERESTS

The authors declare no conflicts of interest arising from the contents of this article.

Received: June 23, 2021
Revised: November 1, 2021
Accepted: November 19, 2021
Published: December 10, 2021

REFERENCES

Adachi, Y., Kato, T., Yamada, T., Murata, D., Arai, K., Stahelin, R.V., Chan, D.C., Iijima, M., and Sesaki, H. (2020). Drp1 tubulates the ER in a GTPase-independent manner. Mol. Cell *80*, 621–632.e6.

Akiyama, H., Iwasaki, Y., Yamada, S., Kamiguchi, H., and Sakakibara, S. (2020). Control of cell migration by the novel protein phosphatase-2A interacting protein inka2. Cell Tissue Res. *380*, 527–537.

Akiyama, H., Nakadate, K., and Sakakibara, S. (2018). Synaptic localization of the SUMOylation-regulating protease SENP5 in the adult mouse brain. J. Comp. Neurol. *526*, 990–1005.

Banker, G. (2018). The development of neuronal polarity: a retrospective view. J. Neurosci. *38*, 1867–1873.

Békés, M., Prudden, J., Srikumar, T., Raught, B., Boddy, M.N., and Salvesen, G.S. (2011). The dynamics and mechanism of SUMO chain deconjugation by SUMO-specific proteases. J. Biol. Biol. Chem. *286*, 10238–10247.

Bellail, A.C., Olson, J.J., and Hao, C. (2014). SUMO1 modification stabilizes CDK6 protein and drives the cell cycle and glioblastoma progression. Nat. Commun. *5*, 4234.

Bertholet, A.M., Delerue, T., Millet, A.M., Moulis, M.F., David, C., Daloyau, M., Arnaune-Pelloquin, L., Davezac, N., Mils, V., Miquel, M.C., et al. (2016). Mitochondrial fusion/fission dynamics in neurodegeneration and neuronal plasticity. Neurobiol. Dis. *90*, 3–19.

Figueroa-Romero, C., Iniguez-Lluhi, J.A., Stadler, J., Chang, C.R., Arnoult, D., Keller, P.J., Hong, Y., Blackstone, C., and Feldman, E.L. (2009). SUMOylation of the mitochondrial fission protein Drp1 occurs at multiple nonconsensus sites within the B domain and is linked to its activity cycle. FASEB J. *23*, 3917–3927.

Fröhlich, C., Grabiger, S., Schwefel, D., Faelber, K., Rosenbaum, E., Mears, J., Rocks, O., and Daumke, O. (2013). Structural insights into oligomerization and mitochondrial remodelling of dynamin 1-like protein. EMBO J. *32*, 1280–1292.

Fukumitsu, K., Hatsukano, T., Yoshimura, A., Heuser, J., Fujishima, K., and Kengaku, M. (2016). Mitochondrial fission protein Drp1 regulates mitochondrial transport and dendritic arborization in cerebellar Purkinje cells. Mol. Cell. Neurosci. *71*, 56–65.

Giacomello, M., Pyakurel, A., Glytsou, C., and Scorrano, L. (2020). The cell biology of mitochondrial membrane dynamics. Nat. Rev. Mol. Cell Biol. *21*, 204–224.

Guo, C., Hildick, K.L., Luo, J., Dearden, L., Wilkinson, K.A., and Henley, J.M. (2013). SENP3-mediated deSUMOylation of dynamin-related protein 1 promotes cell death following ischaemia. EMBO J. *32*, 1514–1528.

Guo, C., Wilkinson, K.A., Evans, A.J., Rubin, P.P., and Henley, J.M. (2017). SENP3-mediated deSUMOylation of Drp1 facilitates interaction with Mff to promote cell death. Sci. Rep. *7*, 1–11.

Hansen, A.H., Duellberg, C., Mieck, C., Loose, M., and Hippenmeyer, S. (2017). Cell polarity in cerebral cortex development-cellular architecture shaped by biochemical networks. Front. Cell. Neurosci. *11*, 176.

Harder, Z., Zunino, R., and McBride, H. (2004). Sumo1 conjugates mitochondrial substrates and participates in mitochondrial fission. Curr. Biol. *14*, 340–345.

Hasegawa, Y., Yoshida, D., Nakamura, Y., and Sakakibara, S. (2014). Spatiotemporal distribution of SUMOylation components during mouse brain development. J. Comp. Neurol. *522*, 3020–3036.

Hickey, C.M., Wilson, N.R., and Hochstrasser, M. (2012). Function and regulation of SUMO proteases. Nat. Rev. Mol. Cell Biol. *13*, 755–766.

Hitoshi, N., Ken-ichi, Y., and Jun-ichi, M. (1991). Efficient selection for high-expression transfectants with a novel eukaryotic vector. Gene *108*, 193–199.

Ishihara, N., Nomura, M., Jofuku, A., Kato, H., Suzuki, S.O., Masuda, K., Otera, H., Nakanishi, Y., Nonaka, I., Goto, Y., et al. (2009). Mitochondrial fission factor Drp1 is essential for embryonic development and synapse formation in mice. Nat. Cell Biol. *11*, 958–966.

Iwata, R., Casimir, P., and Vanderhaeghen, P. (2020). Mitochondrial dynamics in postmitotic cells regulate neurogenesis. Science *369*, 858–862.

Kamitani, T., Kito, K., Nguyen, H.P., and Yeh, E.T. (1997). Characterization of NEDD8, a developmentally down-regulated ubiquitin-like protein. J. Biol. Chem. *272*, 28557–28562.

Kamitani, T., Nguyen, H.P., Kito, K., Fukuda-Kamitani, T., and Yeh, E.T. (1998). Covalent modification of PML by the sentrin family of ubiquitin-like proteins. J. Biol. Chem. *273*, 3117–3120.

Kang, X., Qi, Y., Zuo, Y., Wang, Q., Zou, Y., Schwartz, R.J., Cheng, J., and Yeh, E.T. (2010). SUMO-specific protease 2 is essential for suppression of polycomb group protein-mediated gene silencing during embryonic development. Mol. Cell *38*, 191–201.

Khayachi, A., Gwizdek, C., Poupon, G., Alcor, D., Chafai, M., Casse, F., Maurin, T., Prieto, M., Folci, A., De Graeve, F., et al. (2018). Sumoylation regulates FMRP-mediated dendritic spine elimination and maturation. Nat. Commun. *9*, 757.

Kim, E.Y., Zhang, Y., Beketaev, I., Segura, A.M., Yu, W., Xi, Y., Chang, J., and Wang, J. (2015). SENP5, a SUMO isopeptidase, induces apoptosis and cardiomyopathy. J. Mol. Cell. Cardiol. *78*, 154–164.

Kunz, K., Piller, T., and Müller, S. (2018). SUMO-specific proteases and isopeptidases of the SENP family at a glance. J. Cell Sci. *131*, jcs211904.

Liu, R., and Chan, D.C. (2015). The mitochondrial fission receptor Mff selectively recruits oligomerized Drp1. Mol. Biol. Cell *26*, 4466–4477.

Lomeli, H., and Vazquez, M. (2011). Emerging roles of the SUMO pathway in development. Cell. Mol. Life Sci. *68*, 4045–4064.

Luo, H.B., Xia, Y.Y., Shu, X.J., Liu, Z.C., Feng, Y., Liu, X.H., Yu, G., Yin, G., Xiong, Y.S., Zeng, K., et al. (2014). SUMOylation at K340 inhibits tau degradation through deregulating its phosphorylation and ubiquitination. Proc. Natl. Acad. Sci. U S A *111*, 16586–16591.

Ma, W., and Mayr, C. (2018). A membraneless organelle associated with the endoplasmic reticulum enables 3'UTR-mediated protein-protein interactions. Cell *175*, 1492–1506.e19.

Madan, B., Walker, M.P., Young, R., Quick, L., Orgel, K.A., Ryan, M., Gupta, P., Henrich, I.C., Ferrer, M., Marine, S., et al. (2016). USP6 oncogene promotes Wnt signaling by deubiquitylating Frizzleds. Proc. Natl. Acad. Sci. U S A *113*, E2945–E2954.

Niikura, T., Kita, Y., and Abe, Y. (2014). SUMO3 modification accelerates the aggregation of ALS-linked SOD1 mutants. PLoS One *9*, e101080.

Nishida, T., Tanaka, H., and Yasuda, H. (2000). A novel mammalian Smt3-specific isopeptidase 1 (SMT3IP1) localized in the nucleolus at interphase. Eur. J. Biochem. *267*, 6423–6427.

Nishida, T., and Yamada, Y. (2008). SMT3IP1, a nucleolar SUMO-specific protease, deconjugates SUMO-2 from nucleolar and cytoplasmic nucleophosmin. Biochem. Biophys. Res. Commun. *374*, 382–387.

Parsons, J.T. (2003). Focal adhesion kinase: the first ten years. J. Cell Sci. *116*, 1409–1416.

Pichler, A., Fatouros, C., Lee, H., and Eisenhardt, N. (2017). SUMO conjugation - a mechanistic view. Biomol. Concepts *8*, 13–36.

Prudent, J., Zunino, R., Sugiura, A., Mattie, S., Shore, G.C., and McBride, H.M. (2015). MAPL SUMOylation of Drp1 stabilizes an ER/mitochondrial platform required for cell death. Mol. Cell *59*, 941–955.

Represa, A. (2019). Why malformations of cortical development cause epilepsy. Front. Neurosci. *13*, 250.

Rott, R., Szargel, R., Shani, V., Hamza, H., Savyon, M., Abd Elghani, F., Bandopadhyay, R., and Engelender, S. (2017). SUMOylation and ubiquitination reciprocally regulate alpha-synuclein degradation and pathological aggregation. Proc. Natl. Acad. Sci. U S A *114*, 13176–13181.

Ruthel, G., and Hollenbeck, P.J. (2003). Response of mitochondrial traffic to axon determination and differential branch growth. J. Neurosci. *23*, 8618–8624.

Saita, S., Ishihara, T., Maeda, M., Iemura, S.i., Natsume, T., Mihara, K., and Ishihara, N. (2016). Distinct types of protease systems are involved in homeostasis regulation of mitochondrial morphology via balanced fusion and fission. Genes Cells *21*, 408–424.

Saitoh, H., and Hinchey, J. (2000). Functional heterogeneity of small ubiquitin-related protein

modifiers SUMO-1 versus SUMO-2/3. J. Biol. Chem. *275*, 6252–6258.

Schaffert, L.N., and Carter, W.G. (2020). Do post-translational modifications influence protein aggregation in neurodegenerative diseases: a systematic review. Brain Sci. *10*, 232.

Sharma, P., Yamada, S., Lualdi, M., Dasso, M., and Kuehn, M.R. (2013). Senp1 is essential for desumoylating Sumo1-modified proteins but dispensable for Sumo2 and Sumo3 deconjugation in the mouse embryo. Cell Rep. *3*, 1640–1650.

Shen, C., Ye, Y., Robertson, S.E., Lau, A.W., Mak, D.O., and Chou, M.M. (2005). Calcium/calmodulin regulates ubiquitination of the ubiquitin-specific protease TRE17/USP6. J. Biol. Chem. *280*, 35967–35973.

Takano, T., Funahashi, Y., and Kaibuchi, K. (2019). Neuronal polarity: positive and negative feedback signals. Front. Cell Dev. Biol. *7*, 69.

Tatham, M.H., Jaffray, E., Vaughan, O.A., Desterro, J.M., Botting, C.H., Naismith, J.H., and Hay, R.T. (2001). Polymeric chains of SUMO-2 and SUMO-3 are conjugated to protein substrates by SAE1/SAE2 and Ubc9. J. Biol. Chem. *276*, 35368–35374.

Varejão, N., Lascorz, J., Li, Y., and Reverter, D. (2020). Molecular mechanisms in SUMO conjugation. Biochem. Soc. Trans. *48*, 123–135.

Verma, V., Croley, F., and Sadanandom, A. (2018). Fifty shades of SUMO: its role in immunity and at the fulcrum of the growth-defence balance. Mol. Plant Pathol. *19*, 1537–1544.

Waterham, H.R., Koster, J., Roermund, C.W., Mooyer, P.A., Wanders, R.J., and Leonard, J.V. (2007). A lethal defect of mitochondrial and peroxisomal fission. N. Engl. J. Med. *356*, 1736–1741.

Wen, D., Wu, J., Wang, L., and Fu, Z. (2017). SUMOylation promotes nuclear import and stabilization of polo-like kinase 1 to support its mitotic function. Cell Rep. *21*, 2147–2159.

Yamada, S., and Sakakibara, S. (2018). Expression profile of the STAND protein Nwd1 in the developing and mature mouse central nervous system. J. Comp. Neurol. *526*, 2099–2114.

Yamada, S., Sato, A., and Sakakibara, S. (2020). Nwd1 regulates neuronal differentiation and migration through purinosome formation in the developing cerebral cortex. iScience *23*, 101058.

Zahn, M., Kaluszniak, B., Möller, P., and Marienfeld, R. (2021). The PTP1B mutant PTP1BΔ 2-4 is a positive regulator of the JAK/STAT signalling pathway in Hodgkin lymphoma. Carcinogenesis *42*, 517–527.

Zhang, X., Wang, C., Zhao, D., Chen, X., Zhang, C., Zheng, J., and Liu, X. (2020). Zinc deficiency induces abnormal development of the myocardium by promoting SENP5 overexpression. PLoS One *15*, e0242606.

Zhao, Q., Lu, D., Wang, J., Liu, B., Cheng, H., Mattson, M.P., and Cheng, A. (2019). Calcium dysregulation mediates mitochondrial and neurite outgrowth abnormalities in SOD2 deficient embryonic cerebral cortical neurons. Cell Death Differ. *26*, 1600–1614.

Zhao, X. (2018). SUMO-mediated regulation of nuclear functions and signaling processes. Mol. Cell *71*, 409–418.

Zunino, R., Braschi, E., Xu, L., and McBride, H.M. (2009). Translocation of SenP5 from the nucleoli to the mitochondria modulates DRP1-dependent fission during mitosis. J. Biol. Chem. *284*, 17783–17795.

Zunino, R., Schauss, A., Rippstein, P., Andrade-Navarro, M., and McBride, H.M. (2007). The SUMO protease SENP5 is required to maintain mitochondrial morphology and function. J. Cell Sci. *120*, 1178–1188.

STAR★METHODS

KEY RESOURCES TABLE

REAGENT or RESOURCE	SOURCE	IDENTIFIER
Antibodies		
Rabbit polyclonal anti-pan-Senp5	Proteintech	Cat#19529-1-AP; RRID:AB_10643377
Mouse monoclonal anti-HA-tag	MBL	Cat#M180-3; RRID:AB_1095181
Rabbit polyclonal anti-α-tubulin	MBL	Cat#PM054; RRID:AB_10598496
Rabbit polyclonal anti-α-tubulin	Proteintech	Cat#11224-1-AP; RRID:AB_2210206
Rabbit polyclonal anti-GFP	GeneTex	Cat#GTX113617; RRID:AB_1950371
Mouse monoclonal anti-Myc-tag	MBL	Cat#192-3; RRID:AB_11160947
Rabbit polyclonal anti-tagRFP	Evrogen	Cat#AB233; RRID:AB_2571743
Mouse monoclonal anti-SMI312	Biolegend	Cat#837904; RRID:AB_2566782
Chicken polyclonal anti-GFP	Aves Labs	Cat#GFP-1010; RRID:AB_10000240
Rabbit monoclonal anti-Tom20	Cell Signaling Technology	Cat#42406; RRID:AB_2687663
Rabbit monoclonal anti-Senp3	CST	Cat #5591; RRID:AB_10694546
Chemicals, peptides, and recombinant proteins		
PEI MAX	Polysciences	Cat#24765
RNAiso Plus reagents	Takara Bio	Cat#9108
N-ethyl-maleimide (NEM)	Sigma-Aldrich	E3876; Cas: 128-53-0
MG132	Selleck	Cat#S2619
protein A/G plus agarose IP beads	Santa Cruz Biotechnology	Cat#SC-2003
Blocking One	Nacalai Tesque	Cat#03953
Critical commercial assays		
PrimeScript II cDNA Synthesis Kit	Takara Bio	Cat#6210A/B
TB Green Ex Taq II Mix	Takara Bio	Cat#RR820S
HRP-polymer linked anti-rabbit IgG reagent (ImmPRESS)	Vector Lab	Cat#MP-6401-15
Q5 High-Fidelity DNA Polymerase	NEB Japan	Cat#M0491
Immobilon western HRP substrate	Merck Millipore	Cat#WBKLS0500
Experimental Models: Cell Lines		
HEK293T cells	JCRB	Cat#JCRB9068
Hela cells	JCRB	Cat#JCRB9004
Hela-Drp1-KO cells	Saita et al., 2016	N/A
Neuro2a cells	JCRB	Cat#IFO50081
primary cultured cortical neurons (PCNs)	Yamada et al., 2020	N/A
primary cultured neural stem/progenitor cells (NSPCs)	Yamada and Sakakibara, 2018	N/A
Experimental Models: Organisms/Strains		
Mouse: ICR	SLC	http://www.jslc.co.jp/english/animals/mouse.php
Oligonucleotides		
Senp5L (NM_001357087.1); forward primer, 5′-AGACAGCTGGTAACCAAAGGCT-3′	Eurofins	N/A
Senp5L; reverse primer, 5′-TCCGGCTGGA GAGTGTCACAGT-3′,	Eurofins	N/A

(Continued on next page)

Continued

REAGENT or RESOURCE	SOURCE	IDENTIFIER
Senp5S; forward primer, 5′- AGACAGCTG GTAACCAAAGGCT -3′	Eurofins	N/A
Senp5S; reverse primer, 5′- GTACAAAGG GAGACAGAATACCTTC-3′	Eurofins	N/A
β-actin; forward primer, 5′-GGCTGTATTC CCCTCCATCG-3′	Eurofins	N/A
β-actin; reverse primer, 5′-CCAGTTGGTA ACAATGCCATGT-3′	Eurofins	N/A
Recombinant DNA		
pEGFP-Senp3	Nishida et al., 2000	N/A
pEGFP-Senp5L	Nishida and Yamada, 2008	N/A
pCAG-EGFP-Senp5L	This paper	N/A
pCAG-EGFP-Senp5S	This paper	N/A
pIRES2-mCherry	This paper	N/A
pIRES2-mCherry-Senp5L	This paper	N/A
pIRES2-mCherry-Senp5S	This paper	N/A
pMT-mKO1	MBL/Amalgaam	AM-V0221M
mCherry-Sec61B	Ma and Mayr, 2018	Addgene plasmid # 121160
Myc-Drp1	Fukumitsu et al., 2016	N/A
YFP-Drp1 (human isoform 3)	Guo et al., 2013	N/A
YFP-Drp1-4KR mutant	Guo et al., 2013	N/A
HA-Drp1 (human isoform 3)	Guo et al., 2013	N/A
HA-Drp1-4KR mutant	Guo et al., 2013	N/A
pCAG-HA-Drp1	This paper	N/A
pCAG-HA-Drp1-4KR	This paper	N/A
pcDNA3 HA-SUMO1	Békés et al., 2011	Addgene plasmid # 48966
pcDNA3 HA-SUMO3	Kamitani et al., 1998	Addgene plasmid # 17361
HA-Ubiquitin	Kamitani et al., 1997	Addgene plasmid # 18712
Myc-Ubiquitin	This paper	N/A
Senp5 shRNAs	Akiyama et al., 2018	N/A
Software and algorithms		
ImageJ	National Institute of Health	https://imagej.nih.gov/ij/
R package Version 3.4.2.	R Development Core Team	https://www.r-project.org
cellSens	Olympus	https://www.olympus-lifescience.com/ja/software/cellsens/
FV31S-SW	Olympus	https://www.olympus-lifescience.com/ja/support/downloads/
Fusion-capt	Vilber Lourmat	https://www.garvan.org.au/research/capabilities/molecular-genetics/documents/fusion_manual_2016.pdf
Other		
Thermal Cycler Dice Real Time System III	Takara Bio	Cat#TP950
FV3000	Olympus	https://www.olympus-lifescience.com/en/laser-scanning/fv3000/
Fusion Solo S	Vilber Lourmat	https://www.vilber.com/fusion-solo-s/

(*Continued on next page*)

Continued

REAGENT or RESOURCE	SOURCE	IDENTIFIER
NEPA21 Electroporator	Nepagene	http://www.nepagene.jp/e_products_nepagene_0001.html
Axio Observer	Zeiss	https://www.zeiss.com/microscopy/us/products/light-microscopes/axio-observer-for-biology.html

RESOURCE AVAILABILITY

Lead contact

Further information and requests for resources and reagents should be directed to and will be fulfilled by the lead contact, Shin-ichi Sakakibara (E-mail: sakakiba@waseda.jp).

Materials availability

All materials generated in this study are available from the Lead Contact.

Data and code availability

All data reported in this paper will be shared by the lead contact upon request.

This paper does not report original code.

Any additional information required to reanalyze the data reported in this paper is available from the lead contact upon request.

EXPERIMENTAL MODEL AND SUBJECT DETAILS

Mice

Experiments were approved by the Committee on the Ethics of Animal Experiments of the Waseda University. ICR mice (SLC Japan) were maintained on a 12-hour light–dark cycle. Food and water were available ad libitum. The date of conception was established by the presence of a vaginal plug and was recorded as embryonic day zero (E0). The day of birth was designated as P0.

METHOD DETAILS

Cell culture and transfection

HEK293T, Neuro2a, and HeLa cells were cultured in Dulbecco's modified eagle medium (DMEM) (Fujifilm-Wako) containing 10% fetal bovine serum (FBS) (Biowest), penicillin/streptomycin, and 2 mM L-glutamine (Thermo) in a humidified atmosphere of 5% CO_2/95% air at 37°C. Drp1-deficient HeLa cell line (Drp1 KO Hela) was established by CRISPR/Cas9-mediated genome editing technology and characterized in the previous study (Saita et al., 2016). Primary NSPCs were isolated from the E12 telencephalon (Yamada and Sakakibara, 2018). PCNs were prepared from the cerebral cortex of E16-17 mice (Yamada et al., 2020). Cortices were dissociated using 0.25% trypsin, followed by trituration. Cells were plated on coverslips coated with 0.01% poly-D-lysine (PDL) and incubated in Neurobasal medium (Thermo) supplemented with the B-27 (Thermo) and GlutaMAX (Thermo) in a humidified atmosphere of 5% CO_2/95% air at 37°C. Neurons were processed for immunocytochemistry or western blotting after 3 days, *in vitro*. Cultured cell lines were transfected with plasmids using PEI MAX (Polysciences) complexes with a DNA to PEI MAX ratio of 1:3 w/w (Akiyama et al., 2020). Mouse NSPCs and primary cortical neurons were electroporated using the NEPA21 Electroporator (Nepagene) (Yamada et al., 2020).

Cloning of mouse Senp5 cDNAs

Total RNA was isolated from 10 weeks old C57BL/6 mice brains using the RNAiso Plus reagents (Takara Bio). First strand cDNA was synthesized using the PrimeScript II cDNA Synthesis Kit (Takara Bio) following the manufacturer's protocol. The cDNAs encoding the Senp5 open reading frame (ORF) were amplified by Q5 High-Fidelity DNA Polymerase (NEB Japan) with primer sets based on the predicted sequences of the mouse Senp5 isoforms (GenBank accession numbers: Senp5 short isoform 1 [Senp5S], XR_003951796; Senp5 short isoform 2 [Senp5S2], NM_001357088 and XR_004939194). The primers were as follows: forward primer (common to both isoforms), 5′-TCTCGAGCCAGTTCTCATTATGCATCAG-3′; reverse primer for

short form 1, 5′-ATGGTACCTTCAGTACAAAGGGAGACAG-3′. PCR products were sequenced and cloned into the XhoI/KpnI sites of the pEGFP-C2 expression vector (Takata Bio). Isolated cDNA clones were designated as Senp5S and Senp5S2. The ORF nucleotide sequences were deposited with the GSDB, DDBJ, EMBL, and NCBI under accession numbers LC619058 (Senp5S) and LC619059 (Senp5S2).

Quantitative PCR

Total RNAs from the mouse forebrain were reverse transcribed using the PrimeScript II first strand cDNA Synthesis Kit (Takara Bio) with a random hexamer primer. PCR was performed using the TB Green Ex Taq II Mix (Takara Bio) and the Thermal Cycler Dice Real Time System (Takara Bio) according to the manufacturer's protocol. PCR products were loaded on a 1% agarose gel and visualized to confirm the specificity of each primer set.

Plasmids

pEGFP-Senp3 and pEGFP-Senp5L were provided by Dr. T. Nishida (Mie University, Mie, Japan) (Nishida et al., 2000; Nishida and Yamada, 2008). pIRES2-mCherry-Senp5L and pIRES2-mCherry-Senp5S, from which the *Senp5* and *mCherry* genes were translated from a single bicistronic mRNA, were generated through insertion of the Senp5 ORF into pIRES2-mCherry. The pIRES2-mCherry vector was synthesized by replacing the AcGFP part of pIRES2-AcGFP1 (Takara Bio) with the mCherry sequence. pEGFP and pmCherry expression vectors were purchased from Takara Bio. pMT-mKO1, which expressed mitochondria-targeted CoralHue monomeric orange fluorescent protein (Kusabira Orange; MBL/Amalgaam brand, AM-V0221M), was used for mitochondrial imaging. mCherry-Sec61B (Addgene plasmid # 121160, deposited by Dr. Mayr) (Ma and Mayr, 2018) was used for ER imaging. Myc-Drp1, cloned from mouse, was provided by Dr. M. Kengaku (Kyoto University, Japan) (Fukumitsu et al., 2016). YFP-Drp1 (human isoform 3) and the YFP-Drp1-4KR mutant were provided by Dr. Chun Guo (University of Sheffield, UK) (Guo et al., 2013). Wild-type Drp1 or non-SUMOylatable Drp1-4KR were subcloned into a pCAGGS vector to construct the pCAG-HA-Drp1 and pCAG-HA-Drp1-4KR plasmids. The CAG promoter was used to facilitate upregulation of Drp1 and Drp1-4KR, *in vivo* (Hitoshi et al., 1991). pcDNA3-HA-SUMO1 was a gift from Dr. Guy Salvesen (Addgene plasmids # 48966) (Békés et al., 2011). pcDNA3-HA-SUMO3 and HA-Ubiquitin were gifts from Dr. Edward Yeh (Addgene plasmids # 17361 and #18712) (Kamitani et al., 1997, 1998). Plasmid constructs containing short hairpin RNA (shRNA) cassettes in the pRFP-C-RS vector were purchased from OriGene Technologies. Plasmid-transfected cells expressed shRNA, which was controlled by the U6 polymerase III promoter and RFP fluorescent protein (Akiyama et al., 2018). The silencing effect of the Senp5 shRNAs was established in our previous report (Akiyama et al., 2018). The shRNA sequences were as follows: 5′-GCACTACCAGAGCTAACTCAGATAGTACT-3′ (scrambled non-targeting control), 5′-GCAGGT GAAGCATTTCCAGTGTAATAAGG-3′ (Senp5 shRNA#1), and 5′-CTGGAGCAGACAAATCTGTGAG TAGTGTA-3′ (Senp5 shRNA#2). The shRNA #1 and shRNA #2 target both isoforms of Senp5 mRNA (Akiyama et al., 2018).

In utero electroporation

Pregnant mice were anesthetized with medetomidine, midazolam, and butorphanol (Yamada et al., 2020). Plasmid DNA solution was injected into the lateral ventricle of E14.5 mice through the uterus wall and electroporated using the NEPA21 electric-pulse generator (Nepagene) according to the manufacturer's instructions. Embryos were dissected out from the uteri two days after electroporation. They were then perfused transcardially with saline solution and 4% paraformaldehyde (PFA) in 0.1 M phosphate buffer (pH, 7.4).

Immunoprecipitation and immunoblotting

For immunoprecipitation (IP), cells were washed twice in ice-cold phosphate-buffered saline (PBS) and lysed in ice-cold lysis buffer containing 50 mM Tris-HCl (pH, 7.4), 150 mM NaCl, 2 mM EDTA, 1% NP-40, 20 mM N-ethyl-maleimide (NEM), and protease inhibitors (Complete Mini Protease Inhibitor Cocktail, Sigma-Aldrich) for 30 min at 4°C.

For the ubiquitination assay, cells pretreated with or without 5 μM MG132 for 3 h, thereon washed twice with PBS and lysed in denaturing RIPA buffer containing 1% sodium dodecyl sulfate (SDS), 5 mM EDTA, 10 mM dithiothreitol (DTT), 20 mM NEM, and protease inhibitors. Cell lysates were heated for five min at 95°C, followed by a 10-fold dilution with lysis buffer. Lysates were centrifuged at 15,000 rpm for

10 min. The supernatants were incubated with primary antibody for 60 min. The supernatants with primary antibody were coupled with protein A/G plus agarose IP beads (Santa Cruz Biotechnology) overnight at 4°C. After centrifugation, the beads were washed four times with 0.1% NP40 in PBS. The bound proteins were dissolved with 2× sample buffer (125 mM Tris-HCl, pH 6.8, 4% SDS, 10% sucrose, and 0.01% bromophenol blue). IP samples were resolved on 8% or 10% SDS-PAGE gels and transferred onto Immobilon-P membranes (Merck Millipore) using a semidry transfer apparatus. The membranes were blocked using Blocking One (Nacalai Tesque) for 25 min or 5% skim milk for 60 min at room temperature. After washing with 0.1% Tween 20 in Tris-buffered saline (TBST), the membranes were incubated with primary antibody against GFP (1:2,000, GeneTex, GTX113617), HA (1:10,000, MBL, TANA2), Myc (1:7500, MBL, My3), Senp5 (Proteintech, 19529-1-AP), or α-tubulin (1:2,000, MBL, #PM054; 1:5000, Proteintech, 11224-1-AP) diluted in TBST, for 60 min at room temperature. Membranes were subsequently incubated with horseradish peroxidase (HRP)-conjugated anti-rabbit IgG (1:20,000; Cytiva, NA934) or anti-mouse IgG (1:20,000; Cytiva, NA931) for 60 min at room temperature. Blots were visualized using the Immobilon western HRP substrate (Merck Millipore) and the Fusion Solo S (Vilber Lourmat) or LAS-3000 luminescent image analyzer (FujiFilm). ImageJ and Fusion capt (Vilber Lourmat) were used to quantify band densities.

As the epitope sequence, Senp5 antibody used in the present study works as a pan-Senp5 antibody. Therefore, although Senp5S2 expression in neurons remains obscure, ~75kDa band may contains both Senp5S and S2.

Immunocytochemistry

Cortical neurons and cultured cells were fixed with 4% PFA, permeabilized with 0.1% Triton X-100, and blocked with 10% normal goat serum at room temperature for 60 min. Cells were then incubated with anti-tagRFP (1:1,000, Evrogen, AB233), anti-SMI312 (1:1,000, Biolegend, 837904), and anti-HA (1:1000, MBL, TANA2) at room temperature for 60 min. Primary antibody binding was visualized using the Alexa Fluor-conjugated secondary antibody (1:1500, Thermo). Immunofluorescence images were acquired using 40× objective lenses (NA, 0.75; Zeiss) and a CCD camera (AxioCam MRm, Zeiss) mounted on an inverted microscope (Axio Observer, Zeiss).

Immunohistochemistry

Embryos were fixed by immersion or perfusion in the cardiac ventricle with 4% PFA in 0.1 M phosphate buffer (pH 7.4), followed by post-fixation overnight at 4°C. Fixed embryo brains were cryoprotected in PBS with 30% sucrose overnight at 4°C and embedded in an optimal cutting temperature compound (Sakura Finetek). Frozen sections were cut at a thickness of 14 μm using a cryostat and were collected on MAS coated glass slides (Matsunami Glass). For antigen retrieval, tissue sections were heated at 90 to 95°C for 10 min in 10 mM sodium citrate buffer (pH, 6.0) using a microwave oven, followed by treatment with 0.3% H_2O_2 in PBST (0.1% Triton X-100 in PBS) for 40 min at 25°C to quench endogenous peroxidase activity (Yamada and Sakakibara, 2018). Sections were blocked for an hour in 5% normal horse serum in PBST and incubated overnight at 4°C with primary antibodies diluted in the same blocking solution. Sections were incubated with HRP-polymer linked anti-rabbit IgG reagent (ImmPRESS; Vector Lab) for 2 h. HRP signal was visualized with 0.25 mg/mL diaminobenzidine and 0.03% H_2O_2. Each step was followed by four washes with PBST. Free-floating sections were mounted on glass slides, dehydrated, and coverslipped with Entellan New (Merck Millipore). For control sections, primary antibodies were either omitted or replaced with normal rabbit serum.

For double immunostaining, frozen sections, treated with antigen retrieval solution, were blocked for 2 h at 4°C with 5% normal goat serum in PBST and incubated with anti-GFP (1:2000, Aves Labs, GFP-1010), anti-HA (1:500, MBL, TANA2), and anti-Tom20 (1:300, Cell Signaling Technology, D8T4N) antibody overnight at 4°C. After washing with PBST, sections were incubated with Alexa Fluor 488-, Alexa Fluor 555- (Thermo), or DyLight 549- (Jackson ImmunoResearch) conjugated secondary antibodies [$F(ab')_2$ fragment]. After counterstaining with 0.7 nM Hoechst 33342 (Thermo), sections were mounted and imaged using a confocal (FV3000, Olympus) or fluorescence inverted microscope (Axio Observer, Zeiss).

Analysis of mitochondrial and ER morphology

In mitochondrial morphological analysis, 5–10 z-stack images (1-μm steps) of pMT-mKO1 plasmid-transfected cells were acquired using a confocal microscopy system (FV3000, Olympus). Deconvolution was applied to maximum projection images to clarify the mitochondrial contours. Mitochondrial length was

defined as the longitudinal axial length of each mitochondrial fragment, which were traced with cellSens life science imaging software (Olympus). Mitochondrial length was calculated as the mean length of mitochondria within a single cell.

In ER morphological analysis, mCherry-Sec61B-expressing cells were kept in a humidified atmosphere at 37°C using a Stage Top incubator (Tokai-hit). Live cell images were acquired using the confocal microscopy system (FV3000, Olympus). The standard deviation (SD) and mean of the fluorescence intensity were obtained using line-scan analysis by the FV31S-SW (Olympus) in a randomly selected cell region. The ER morphology was defined as reticular when the coefficient of variation (CV) scores (SD/mean) were >0.2.

Analysis of co-localization

For co-localization analysis of mitochondria or ER with Drp1, Drp1-KO HeLa cells expressing mCherry-Sec61B or pMT-mKO1 and YFP-Drp1-WT or YFP-Drp1-4KR were grown in a Stage Top incubator (Tokai Hit) at 37°C in a humidified atmosphere. Live cell images were acquired using a confocal microscope system (FV3000, Olympus). For co-localization analysis, Pearson's correlation coefficient and fluorescence intensity were measured using cellSens life science imaging software (Olympus). There were no statistical differences in mCherry or mKO fluorescence intensity between HeLa cells expressing Drp1-WT and Drp1-4KR. Correlation coefficients were Fischer z-transformed and subjected to statistical analysis.

QUANTIFICATION AND STATISTICAL ANALYSIS

Statistical analysis

Statistical analyses were performed using the R package Version 3.4.2. Welch's *t*-test, Wilcoxon rank sum test, or the Chi-square test was used to compare two groups. Two-way ANOVA was used to examine the interaction effects. The P value was corrected using the Holm-Bonferroni correction when there were three or more groups. *, $P<0.05$; **, $P < 0.01$; ***, $P < 0.001$ were considered statistically significant.

iScience, Volume *24*

Supplemental information

Drp1 SUMO/deSUMOylation by Senp5 isoforms influences ER tubulation and mitochondrial dynamics to regulate brain development

Seiya Yamada, Ayaka Sato, Naotada Ishihara, Hiroki Akiyama, and Shin-ichi Sakakibara

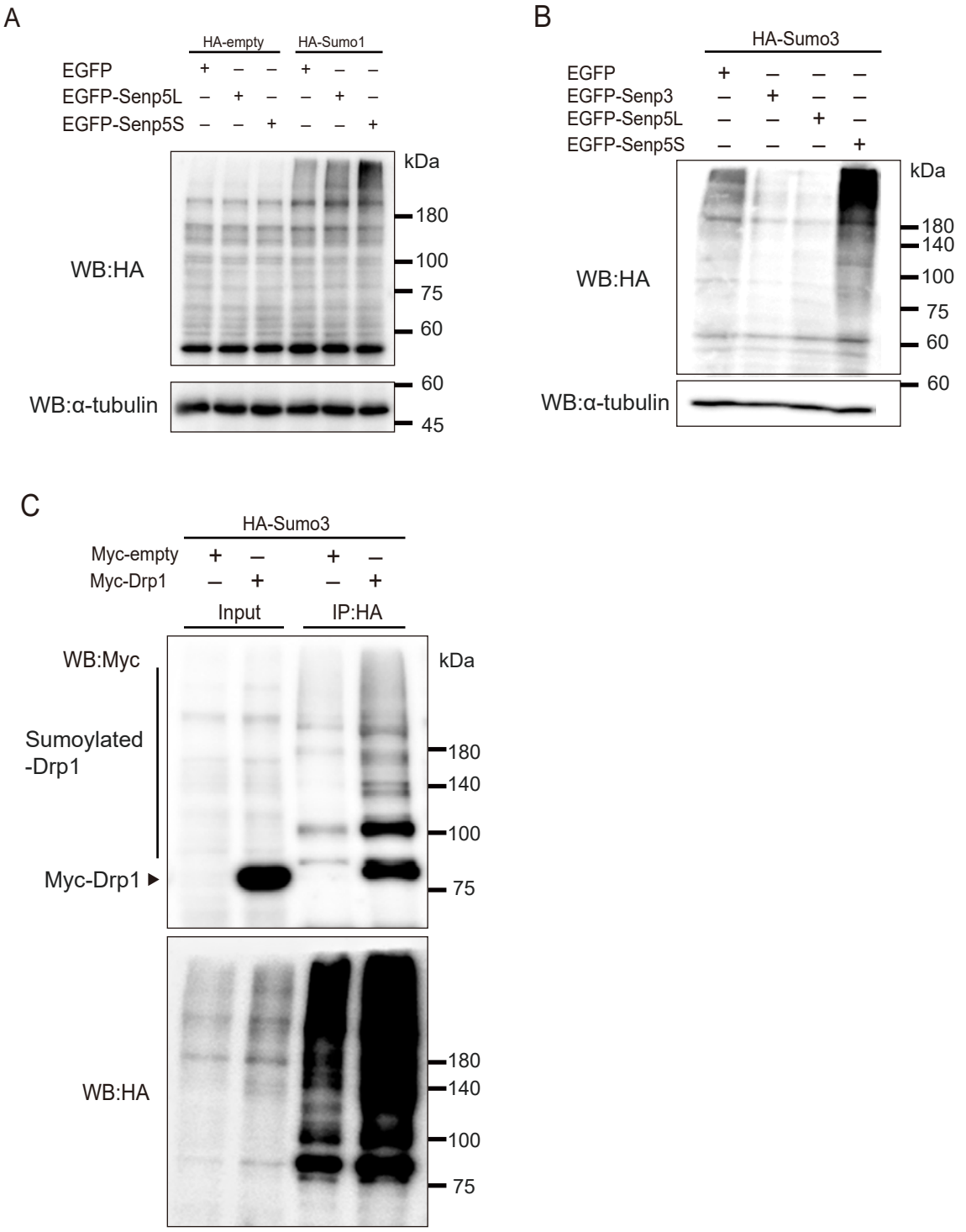

Figure S1. Senp5S promotes SUMOylation (Related to Figure 2)
(A) HEK293T cells were transfected with EGFP, EGFP-Senp5L, or EGFP-Senp5S along with HA-empty vector or HA-SUMO1, followed by immunoblotting with anti-HA (upper panel) or anti-α-tubulin (bottom panel).
(B) Neuro2a cells were transfected with EGFP, EGFP-Senp3, EGFP-Senp5L, or EGFP-Senp5S along with HA-SUMO3, followed by immunoblotting with anti-HA (upper panel) or anti-α-tubulin (bottom panel).
(C) HEK293T expressing Myc empty vector, or Myc-Drp1 along with HA-SUMO3 were immunoprecipitated (IP) with anti-HA antibody. Total cell lysates (input) or IP samples were analyzed by immunoblotting with anti-Myc (upper panel) and anti-HA (bottom panel).

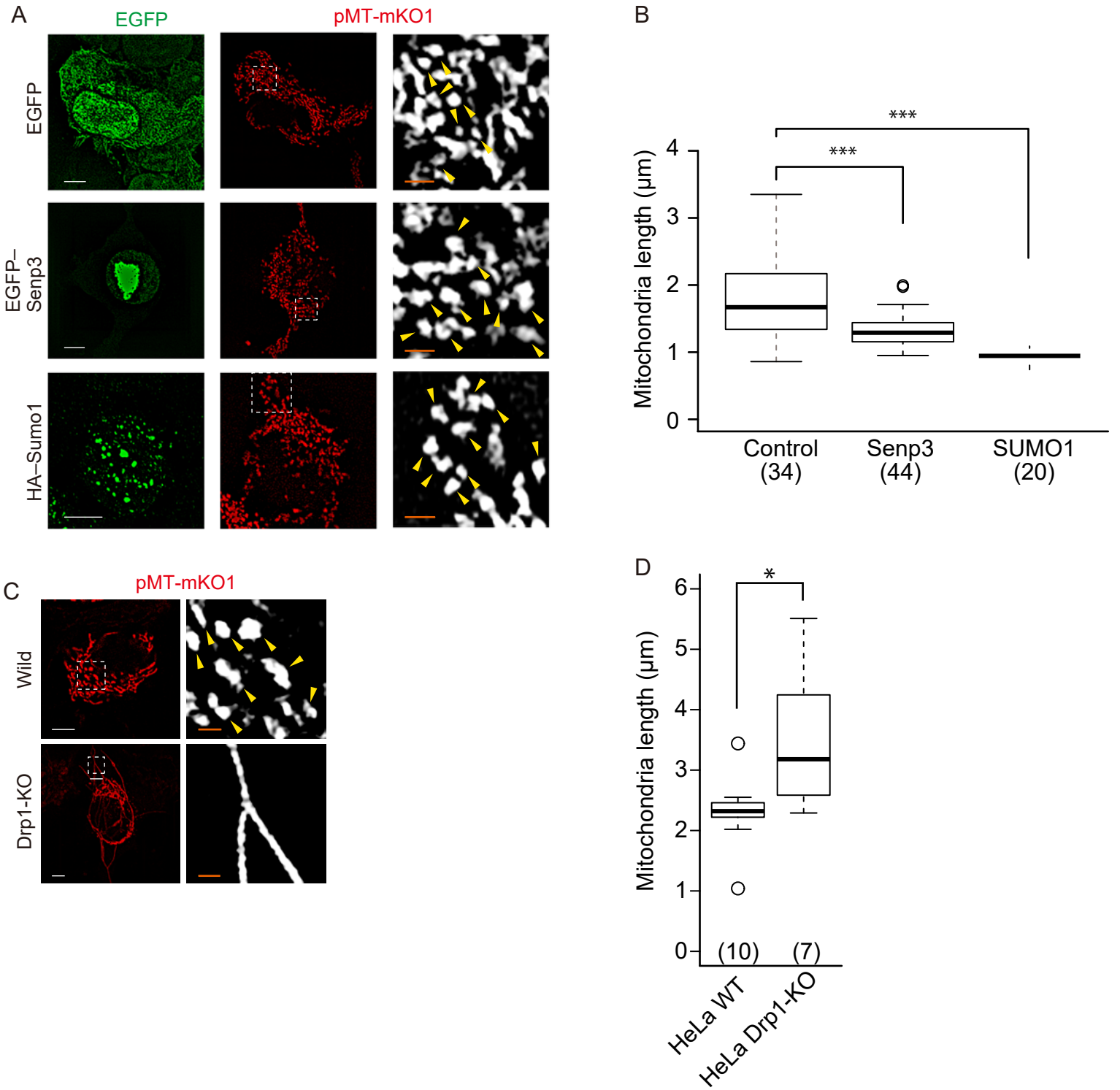

Figure S2. SUMO conjugation to Drp1 adjusts mitochondrial dynamics (Related to Figure 3)
(A, B) HEK293T cells were co-transfected with EGFP-Senp3 or HA-SUMO1 together with pMT-mKO1, followed by immunocytochemistry with an anti-HA (green). Higher magnification of the boxed areas shows pMT-mKO1+ mitochondrial morphology (white). Arrows (yellow) denote fragmented mitochondria. (B) The box and whisker plots summarize the mitochondrial length (μm). Numbers in parentheses indicate the numbers of cells measured. ***, $P < 0.001$; Welch's t-tests with Holm-Bonferroni correction.
(C, D) Confocal images of wild-type or Drp1-KO HeLa cells. pMT-mKO1 (red) was transfected to visualize mitochondrial morphology. Right column, magnified views of the boxed areas showing individual mitochondria (gray-scale). Arrowheads indicate fragmented mitochondria. (D) Box and whisker plots summarize the mitochondrial length (μm). Numbers in parentheses indicate the numbers of cells measured for mitochondrial length determination. *, $P < 0.05$; Welch's t-test.
Scale bars, 5 μm in (A) and (C), and 1 μm in the magnified view.

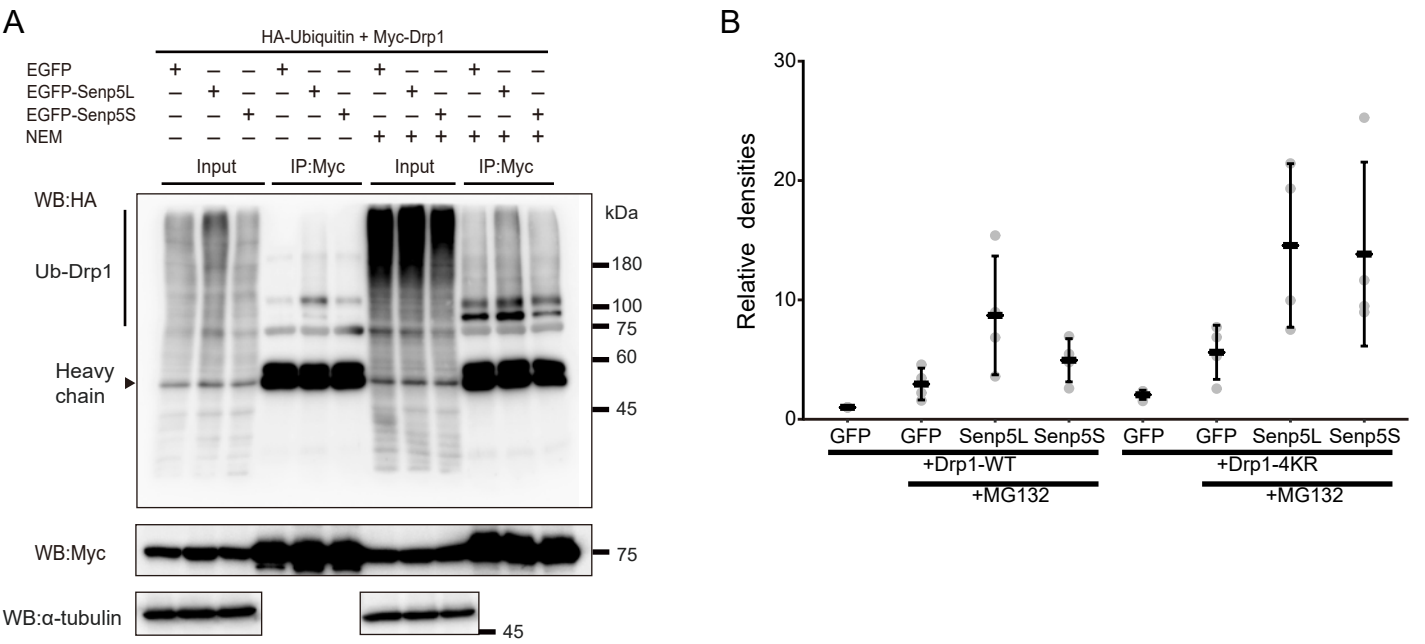

Figure S3. Drp1 deSUMOylation promotes NEM dependent ubiquitinations (Related to Figure 4) (A) HEK293 cells expressing EGFP, EGFP-Senp5L, or EGFP-Senp5S together with Myc-Drp1 and HA-SUMO3 were subjected to immunoprecipitation with an anti-HA antibody with ± N-ethyl-maleimide (NEM), followed by immunoblotting with anti-HA or anti-Myc antibodies. (B) Quantified comparison of the effect of EGFP, Senp5L, or Senp5S along with Drp1-WT or Drp1-4KR on Ub-Drp1 in figure 4A. Total chemiluminescent densities above 100kDa were measured and normalized by that of control, i.e., EGFP and Drp1-WT in the absence of MG132. Gray dots represent four independent experiments. Mean ± SD are also shown.

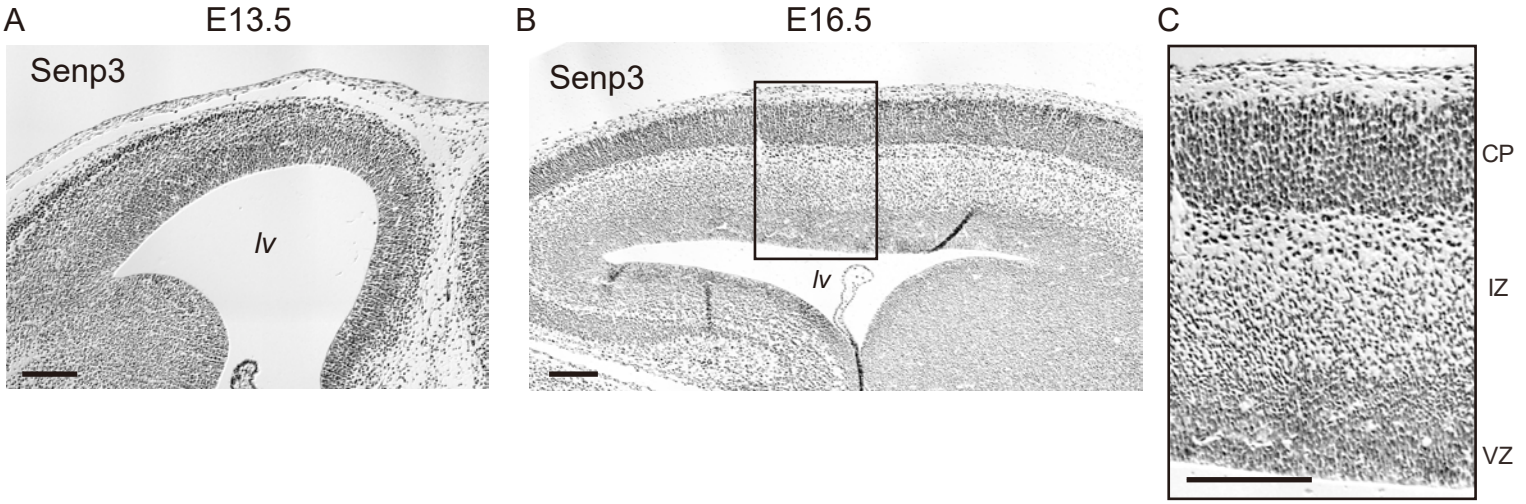

Figure S4. Senp3 expression in the developing cortex (Related to Figure 5)
(A–C) Coronal sections of the cerebral cortex at E13.5 (A) and E16.5 (B) immunostained with an anti-Senp3 antibody. (C) Higher magnification of the area of the cerebral cortex surrounding the lateral ventricle (lv) in B. Scale bars, 100 μm in (A, B); 25 μm in (C). lv, lateral ventricle; CP, cortical plate; IZ, intermediate zone; VZ, ventricular zone.

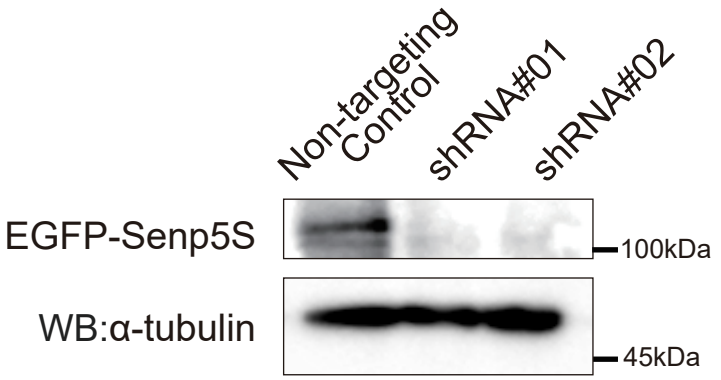

Figure S5. Validation of Senp5 shRNAs against Senp5 (Related to Figure 5)
Neuro2a cells were transfected with pCAG-EGFP-Senp5S and two different mouse Senp5 shRNA constructs (shRNA #01 and shRNA #02) or a non-targeting control shRNA, followed by immuno-blotting with an anti-GFP or anti-α-tubulin antibody.